COMPUTATIONAL FLOW ANALYSIS OF A FLAPPING MICRO-FLYER WING FOR CYCLE-AVERAGED FORCE PRODUCTION

by

NITESH RAJENDRA RAJPUT

Presented to the Faculty of the Graduate School of
The University of Texas at Arlington in Partial Fulfillment
of the Requirements
for the Degree of

MASTER OF SCIENCE IN MECHANICAL ENGINEERING

THE UNIVERSITY OF TEXAS AT ARLINGTON

December 2014

To my parents,

Gita and Rajendra Rajput

I am who I am today because of you both

ACKNOWLEDGEMENTS

Supremely, I praise the Almighty GOD for his blessings, protection and guidance.

The dissertation could not have been completed without the exceptional guidance of my supervisor, Dr. Brian H. Dennis, Associate Professor at Mechanical & Aerospace Engineering, UTA. For me, he is a pantomath. He has always been a one stop solution for all the problems in my research.

I owe my deepest gratitude to my mentor, Alok A. Rege. I would be completely lost in the jungle of CFD if he was not there to save me at all stages of my research. He has made available his support in a number of ways. He was ready to help me from the day I stepped in the CFD Lab till my thesis dissertation. He taught me how to deal with problems and was ready to direct me even in middle of his own research.

I would like to thank other members of my committee, Dr. Zhen X. Han and Dr. Bo P. Wang for showing solemn interest in my research. I am also grateful to fantastic MAE staff and specially, Debi O. Barton who helped me altruistically in the past two years.

It is an honor for me to be a part of Computational Fluid Dynamics Laboratory (CFD lab). Special thanks to all my lab friends who have contributed to the progress I have made. I would like to thank James Grisham for his undisputed programming skills, he made my life easy by automating a lot of functions with his scripts.

I further extend my thanks to Dr. Nilakshi Veerabathina, my advisor who understood me more as a colleague than as a boss. She respected my research and motivated me to balance my job and studies.

I am indebted to my brother, Bhavesh, and sister-in-law, Hinal, who trusted in me and encouraged me at every step along the way. You have been continually supportive for my education. Thanks for listening to my problems and providing perspective and solutions.

A special thanks to uncle and aunt, Ashok and Rajeshri Ranchchod and their family for ensuring I don't feel homesick in this foreign land.

I cannot forget the people who were always there to cheer me and boost my mood when I was low and needed someone to talk to, my friends. This is to all my Katta and 46 Gang and special ones who tolerated my tantrums and were still on my side.

As always, I've saved the best for last. The two souls who shaped me into who I am - Mummy and Pappa. Thank you for the little things you've done for me and for your unconditional love and support.

November 24, 2014

ABSTRACT

COMPUTATIONAL FLOW ANALYSIS OF A FLAPPING MICRO-FLYER WING FOR CYCLE-AVERAGED FORCE PRODUCTION

NITESH RAJENDRA RAJPUT, M.S.

The University of Texas at Arlington, 2014

Supervising Professor: Brian H Dennis

Human engineers have been trying long to mimic creations of nature for their own benefits. One such area of interest is the insect based micro flapping wing flyers for their wide employment in commercial as well as military applications. These micro air vehicles (MAVs) are capable of performing acts that can be too dangerous for humans to perform, such as tactical reconnaissance in a combat zone. The maneuverability required of these MAVs call for a careful design and thorough study of their aerodynamic performance.

This research goal is to provide an estimation of the forces generated during the flapping motion of an airfoil. The commercial computational fluid dynamics software package ANSYS Fluent was used to compute the unsteady forces on a flapping airfoil for different flapping cycle paths. Time averaged forces were then computed from the instantaneous results. A grid independence study was performed to decide the suitable dimension of the grid. Different methods for dealing with the moving boundary were evaluated using mesh deformation and remeshing for unstructured grids.

There is also a need to validate the results obtained from computational analysis. A part of this work concentrated on the validation of ANSYS Fluent results with published experimental data for the unsteady pitching NACA 0012 airfoil.

As an application of the computational model, a sensitivity analysis of various parameters like the Strouhal Number, Reynolds Number, Geometric function, and stroke angle of attack was done to see the effects of these factors in the force generation using Design of Experiments (DOE).

TABLE OF CONTENTS

LIST OF ILLUSTRATIONS

LIST OF TABLES

NOMENCLATURE

α	Pitch angle
α_P	Angle of attack for pitching airfoil (deg)
α_S	Stroke angle of attack
μ	Dynamic Viscosity (kg/m-s)
ω	Wing flapping frequency
ρ	density (kg/m^s)
c	chord (m)
C_{Davg}	Average drag co-efficient
C_D	Drag co-efficient
C_{Lavg}	Average lift co-efficient
C_L	Lift co-efficient
C_N	Normal lift co-efficient
C_{Xavg}	Average horizontal force co-efficient
C_X	Horizontal force co-efficient
C_{Zavg}	Average vertical force co-efficient
C_Z	Vertical force co-efficient
G	Geometric function
L	Wing semi-span
M	Mach Number
Re_l	Local Reynolds number
Re_f	Free Stream Reynolds number
St	Strouhal number

t	time(secs)
V_f	Free stream speed (m/s)
V_l	Local speed (m/s)

CHAPTER 1

INTRODUCTION

1.1 The Historic Odyssey of Flapping Flight

Insects are the reason there are humans! Surprised? As quoted by Michael Dickinson, American fly-bioengineer in his TED talk at Caltech, "Without insects, there'd be no flowering plants. Without flowering plants, there would be no clever, fruit-eating primates doing research." This research runs far back to when our ancestors were captivated with the flight of birds. It is unquestionable that pre-historic man must have dreamt of flying way before the Greek epics. When civilizations developed, men and women conceived gods in the sky with wings. Thus, no matter what ancient civilization one looks at, its gods could fly. But until the not-so-distant past, human flight was but a figment of imagination. Attempts were made to mimic birds, but this idea was ahead of its time [fig 1.1]. If we take a look at history when gossamer wings crafted in ancient mythology by Daedalus and Icarus [fig 1.2] to the Ornithopter [figures:1.3(a), 1.3(b)]based on Leonardo da Vinci's drawings during the renaissance, they all mimicked the flapping of wings and attempted to adapt it for human use.

Intellects of medieval and renaissance period attributed the power of wings to produce lift to psychic and mysterious forces possessed by birds. This view held that flying required not an understanding of natural laws, but rather their circumvention through the conjuring of magical powers. As mentioned by Charles H. Gibbs-Smith in his book Aviation: An Historical Survey, these misconceptions were proved wrong in seventeenth century when scientists like Aristotle and Archimedes conceptualized

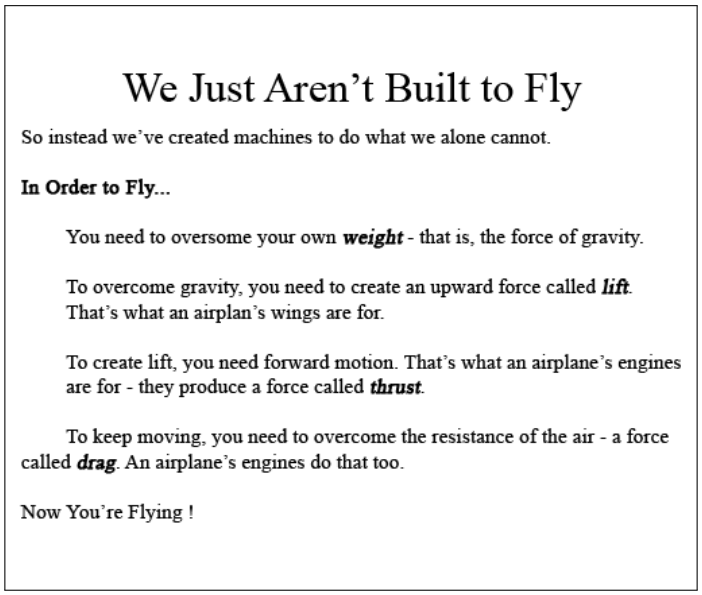

Figure 1.1. Why humans can't fly?(Image: National Air And Space Museum).

terms like drag and pressure gradients. In 1726, Sir Isaac Newton became the first person to develop a theory of air resistance. George Cayley, in 1799 discovered the four aerodynamic forces of flight: weight, lift, drag, and thrust. thrust. He also elucidated the relationship between them.

1.2 Insect Flapping Flight

The flapping motion of wings is used in the powered flight of birds and insects to counter the gravity force and propel them against aerodynamic drag. All birds and insects use this flapping motion to generate the forces with certain differences, for instance, in birds, the Reynolds number (Re) and the wing aspect ratio is higher than in insects. Also, birds use their wings to sustain their weight by lift while insects use high frequency and different flapping trajectories to maximize C_L/C_D ratio for long range flight or $C_L^{3/2}/C_D$ ratio for long-duration flights [1].

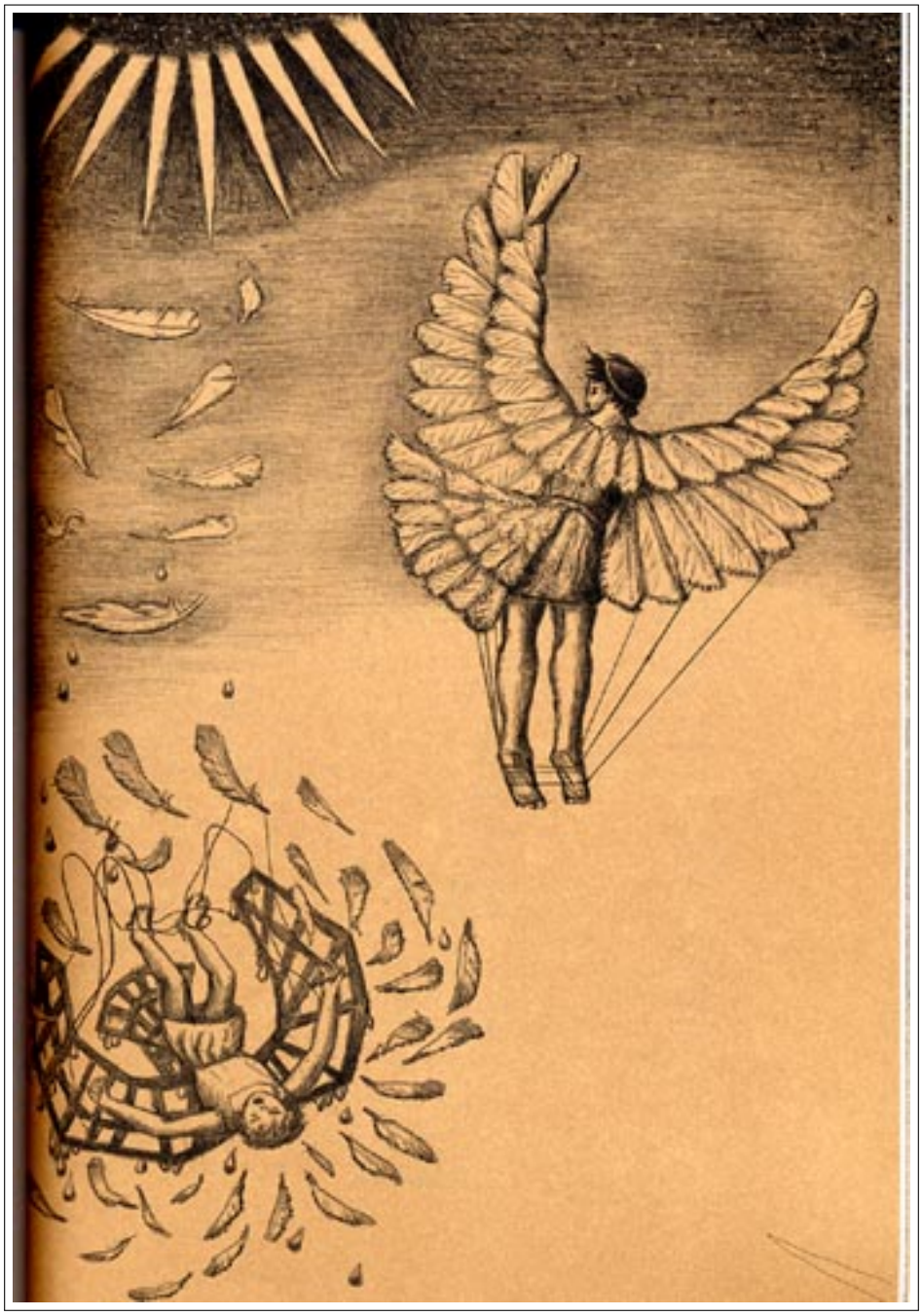

Figure 1.2. Greek mythological characters - Icarus and Daedalus attempt to fly using wings of feather and wax (Image: www.passionweiss.com/category/daedelus/).

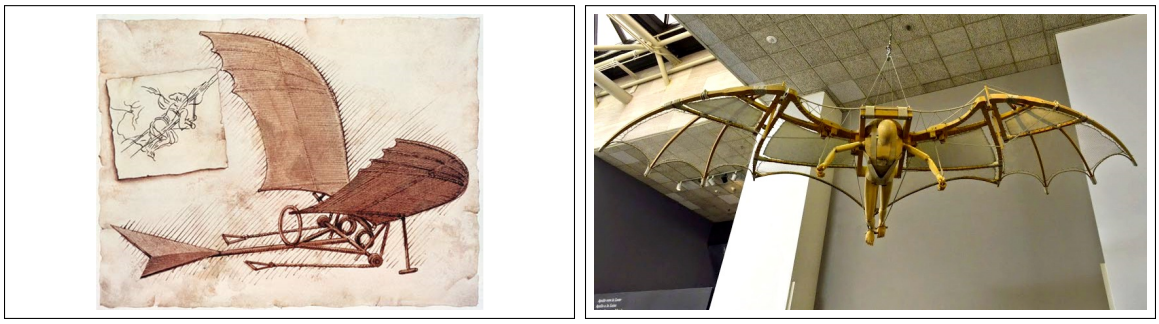

(a) (b)

Figure 1.3. Da Vinci's Ornithopter fig (a)Drawing in the Codex(Image: www.britannica.com) and fig (b) Model of Ornihopter in National Air And Space Museum in Washington D.C.(Image: Personal Capture).

The flight of insects is of keen interest to the researchers and to us in this research because of their extraordinary evolutionary success of flight. Also, because their survival and evolution depend so crucially on flight performance, different flight related sensory, physiological, behavioral and biomechanical traits of insects are among the most compelling illustrations of adaptations found in nature.

The flapping motion of an insect can be decomposed into three separate motions: sweeping or flapping (forward and backward movement of wings), heaving (up and down movement) and pitching (changing incidence angle). In fig 1.4, a schematic representation of left wing motion of an insect is shown. A complete flap cycle for a complete insect wing motion consists of two translations (a downstroke and an upstroke) and two rotations (termed pronation at the end of the down-stroke and supination at the end of the up-stroke). During the translation, the wing may show sweeping, heaving and pitching motions. In addition to that, at the end of a half-stroke during stroke reversal (rotation) the wing pitches rapidly. The exact wing kinematics varies among different insects and for different motions in flight. Insects may change their stroke angle, angle of attack and wing rotation to perform desired flight maneuvers [2].

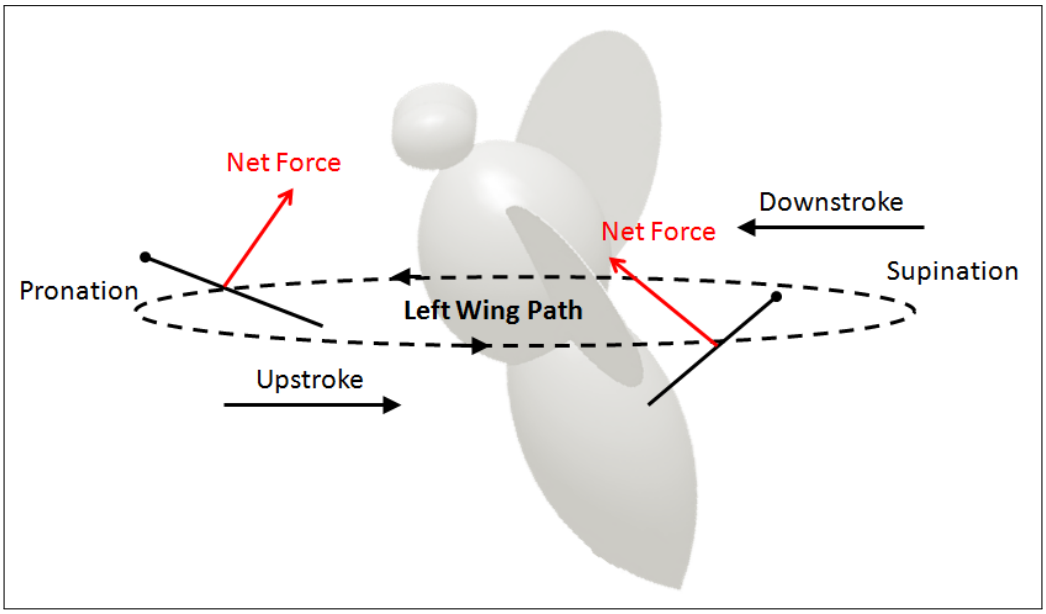

Figure 1.4. Insect wing motion (left wing). The black lines denote the instantaneous position of the wing cross-section. The solid circle denotes the wing leading edge (Image taken from[1]).

1.3 Micro Air Vehicles

Micro Air Vehicles (MAV) are a class of Unmanned Air Vehicles (UAV) with length scale similar to birds and insects. The term, MAV, may be deceptive to many people if translated literally. We might ideate these flying models to be miniature or small versions of larger aircraft because of the term micro in MAV. Fig 1.5 gives a canonical representation of the definition of MAVs. Defense Advanced Research Project Agency (DARPA) defined these flyers to a size less than 15cm (about 6 inches) in length, width and height.They fly at relatively low speeds (usually less than 30 mph or 42.28 kmph). These are affordable, fully functional, military capable and small flight vehicles. Their applications range from military to commercial uses like reconnaissance, surveillance, targeting, tagging, pollination, traffic monitoring, fire and rescue and real-estate photography to name a few.

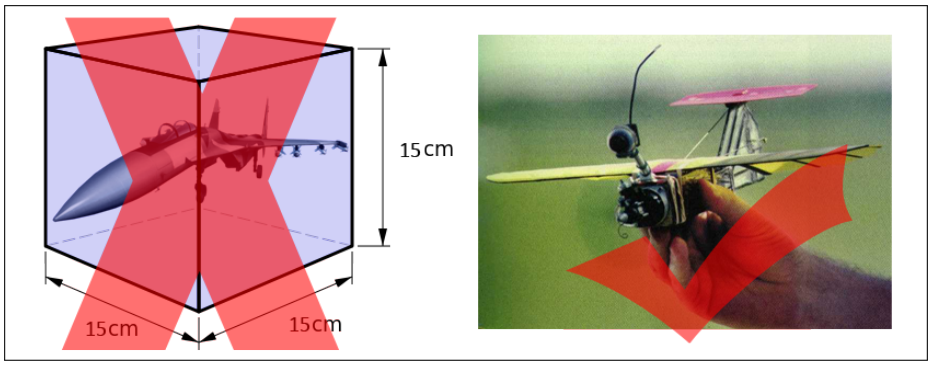

Figure 1.5. Micro Air Vehicle - Definition.

MAV can be of different types: fixed-wing aircraft, rotary-wing aircraft, or flapping-wing; with each being used for different purposes. The flapping-wing MAVs are bio-inspired and they mimic the motions of insects. This research is concentrated on flapping wing bio-inspired micro air vehicles.

1.4 Literature Review

This work was started with an aim to solve the problem faced by Rege et al. [1, 3, 4] where they performed a parametric study to understand the effects of various parameters on force generation. Author presented the solutions for the remeshing and grid adaptation issues. Analytical expressions for estimation of the forces on the wings of various insects and the work and power produced were presented by Weis-fogh [5] in his seminal paper. The cycle-averaged aerodynamic forces were presented by Wood in [6] with reference to Sane et al. [7]. Difficulties encountered using computational modeling of aerodynamic forces was summarized by Shyy et al. in [8]. Jane Wang in [9] proved, using computational methods, that a two dimensional hovering motion can generate enough lift to support a typical insect weight while Sun et. al in [26] solved the Navier-Stokes equations numerically and examined the lift and power requirements of hovering insect flight. Theory on Drosophila wings

put forward by Dickinson et. al was verified by Ramamurti in [10]. They employed a finite element flow solver to compute an unsteady flow past 3-D Drosophila wing undergoing flapping motion.

1.5 Organization of Report

The following thesis report exhibits the research details by dividing it into different chapters.

Chapter one gives brief introduction of flapping flight, its background and the applications. This chapter also presents the aims and objectives of the research and also a general overview on the research area.

The different 2D and 3D models used in the research are described in chapter two.

Implementation of CFD approach for solving the fluid flow is explained in detail in chapter three. The setup and working of ANSYS Fluent 14.5.7 is also explicated in this chapter.

In chapter four, grid generation and the different wing trajectories used in the research has been described.

In chapter five and six, research methodology has been discussed step-by-step, which gives the description for the grid independence study and the experimental validation of the CFD results respectively. Chapter seven deals with the application in sensitivity analysis using design of experiments for figure-8 flapping path. Each of these chapters conclude with their respective results.

Chapter eight gives the conclusions on the research and the recommendations for future research.

1.6 Aim of Research

1.6.1 Aim

The aim is to computationally analyze the flow over a flapping micro-flyer wing for cycle-averaged force production.

1.6.2 Objectives

- Obtain the best size of the grid for flow using grid independence study.
- Validate the CFD results with experimental results.
- Accurately represent forces involved in flapping wings.
- Extend the study in third dimension.

CHAPTER 2

MODEL

2.1 Bio-Inspired Work

There has been an extensive research on bio-inspired flight using different insects. A deep study on diptera insects was done by Weis-Fogh [5] and Ennos [11]. Azuma et al. [12] in their research studied the flight mechanics of a Dragonfly, while Tobalske et al. in [13] concentrated on Hummingbird flight. Sun [14, 15], Bai [16] and Zanker [17] chose Drosophila melanogaster for their research. There has also been intensive study on insects for their flapping wing phenomenon. Dickinson [18] used a dynamically scaled model of Drosophila melanogaster for the experimental research. Rege et al. is working on his research on the flapping wing flight study inspired by the insects. This work is an extension of the research done by Rege et al.. The model of the flapping wing used in this study is same as that used for his Masters Thesis.

2.2 Flapping Wing MAV Model

The flapping wing micro-flyers are inspired from birds or insects. The wings for this study are inspired from insects as shown in fig 2.2 and are modeled as thin elliptical plates with variable chord as shown in fig 2.1. This study is concentrated only on the micro-flyer wings.

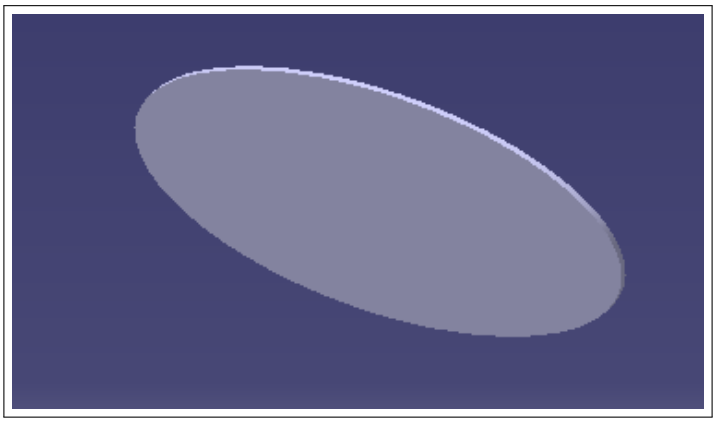

Figure 2.1. Flapping wing model.

Figure 2.2. Bio-inspired MAV.

2.3 Wing Models

2.3.1 For 3D Flapping

The wing model as discussed above would be in the 3D straight flapping path motion study. The minor to major axis ratio of the model was 0.4 and the thickness of the plate is 0.01 units as shown in the fig 2.3 The root of the wing is fixed at (-0.00571, 0, 0.3427). The straight path trajectory of the wing is about the root.

2.3.2 For Grid Independence Study and Sensitivity Analysis

The study in three dimensions comes with a lot of intricacies. So, we decided to restrict the initial study to two dimensions. A cross section of the thin elliptical plate of length 1 mm and thickness 0.01 mm was taken and a study on 2D flat plate model was done as a major part of this study. Sensitivity analysis and parametric

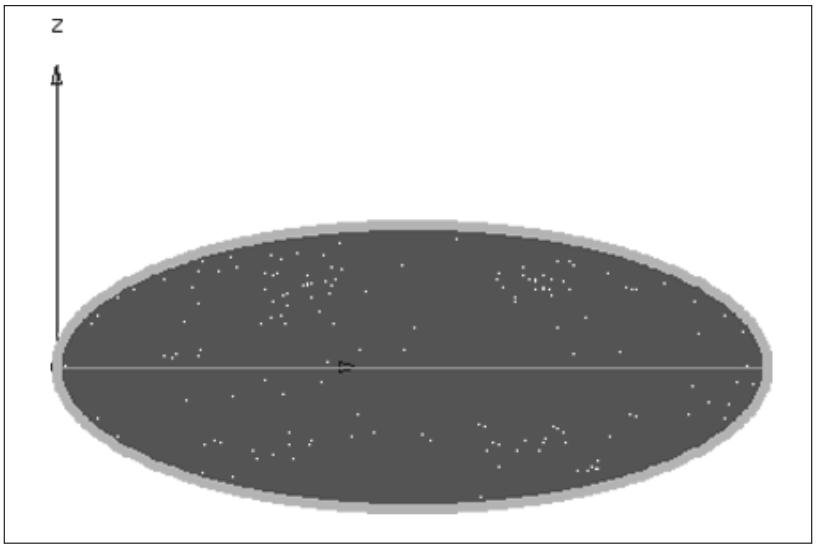

Figure 2.3. 3D Thin Elliptical plate.

study using design of experiments (DOE) was done simulating the 2D cross section as shown in fig 2.4. The two edges of the model were blunted to avoid flow detachment. The model was placed with its center coinciding with the origin of the workspace coordinate system for the sensitivity analysis. While the center of the model was shifted to x = 1.414 and y = -0.400 in the parametric study to compensate for the motion of the wing.

2.3.3 For Experimental Validation

A standard NACA 0012 airfoil section of unit chord length was used for the validation study. This airfoil was chosen to simulate the experiments by AGARD [19] (Advisory Group for Aerospace Research and Development) where 12 percent thick symmetrical airfoil was used. The center of the workspace coincided at 0.25c of the model since the pitching motion was about quarter-chord as shown in fig 2.5

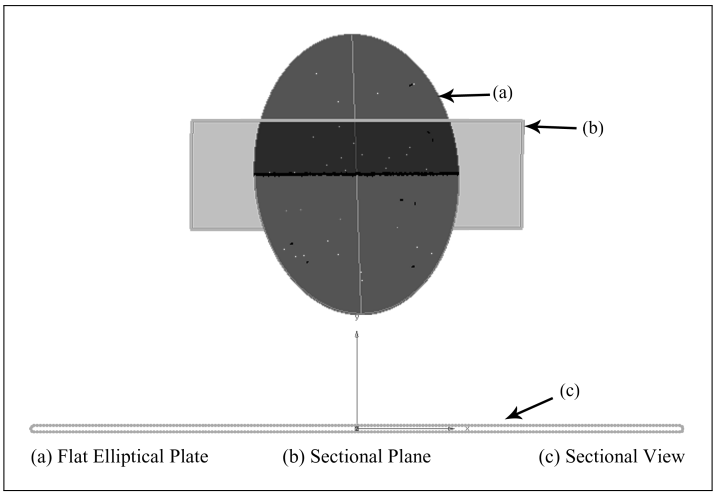

Figure 2.4. Wing sectional model as seen in X-Y plane .

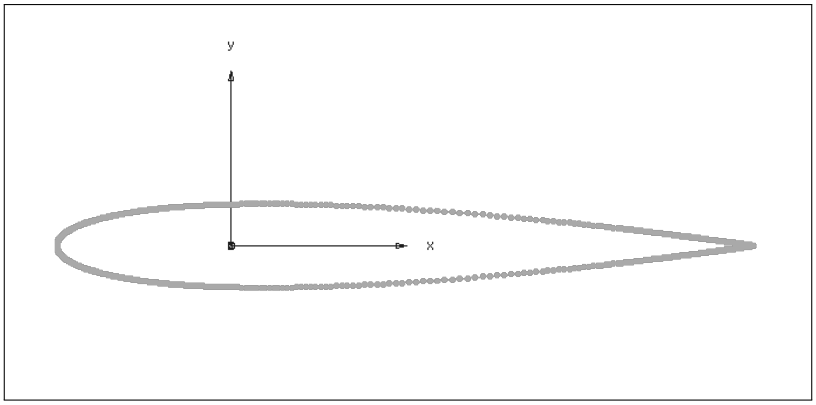

Figure 2.5. NACA 0012 airfoil section.

CHAPTER 3

COMPUTATIONAL FLUID DYNAMICS

3.1 Introduction

Computational fluid dynamics (CFD) is an approach of numerically solving the governing equations describing a fluid flow by means of computer based simulation. In this approach, a limited number of assumptions are made and a high speed computer is used to solve the resulting governing fluid dynamic equations. This technique can be a medium to simulate flow conditions which is an alternative to the experimental approach, which is often restrained by high costs in design, model scaling problems, measurement difficulties and reduced lead times. CFD tools are the computer applications or the software developed by applying laws of fluid dynamics and fundamental mathematical equations to solve the various fluid flow problems as in fig 3.1.

3.2 ANSYS Fluent 14.5.7 - CFD Tool

ANSYS Fluent (later referred to as Fluent) is a commercial computer program written in the C language for modeling fluid flow, heat transfer, and chemical reactions in complex geometries. Fluent uses a client/server architecture, which enables it to run as separate simultaneous processes on client desktop workstations and powerful computer servers, this feature of Fluent is used to its full extent in this research and Grendel is used to run the simulations of Fluent.

Grendel as seen in fig 3.2 is a Linux only machine in UTA CFD Laboratory with a total of 54 processors and 13.5 GB of core memory. Each of the nodes has a 3COM EtherLink 905B 100 Mb/sec fast ethernet adapter except the two Xeon base

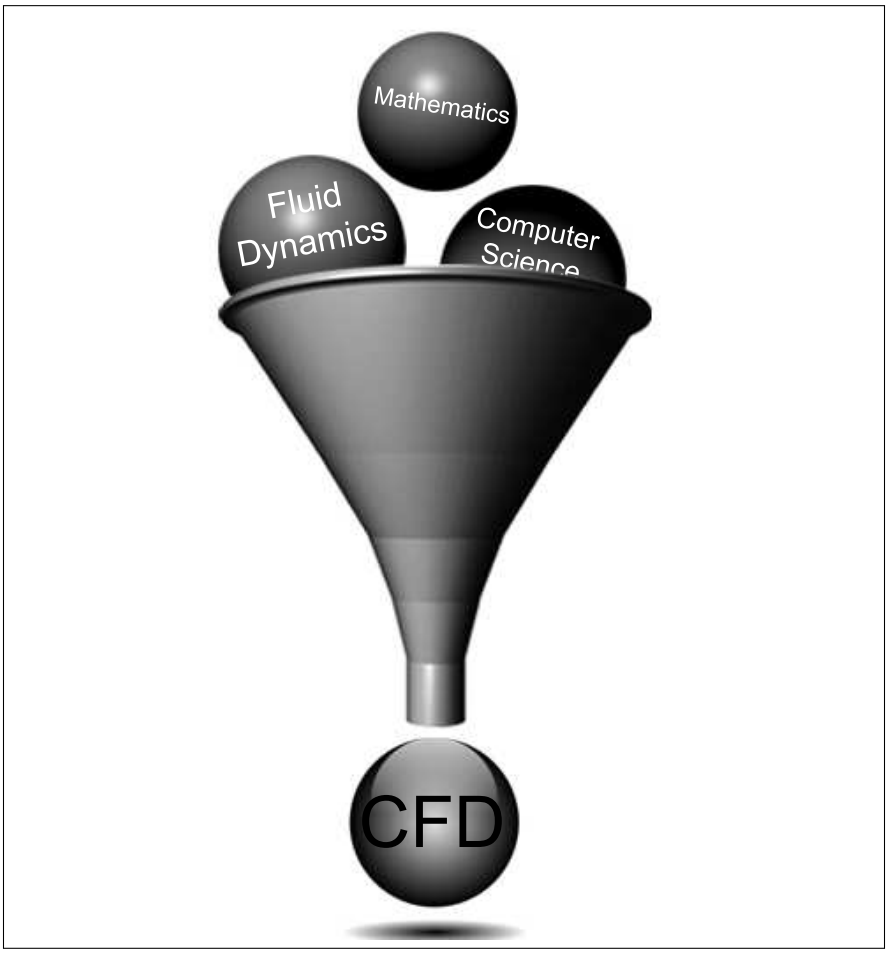

Figure 3.1. Symbolic representation of CFD approach.

nodes which use the Intel fast ethernet adapter on the SuperMicro motherboard. A Baystack 450 fast Ethernet switch with a 4-port MDA expansion module is used for network switching.

3.2.1 Solver

There are two solvers available in the software package: Pressure-based and density-based. The pressure-based solver is used for incompressible and mildly compressible flow while the density-based solver is used for high-speed compressible flows. In this research, the pressure-based solver is used since the study is focused on the in-

Figure 3.2. Grendel machine in UTA CFD laboratory.

compressible flow. The two algorithms under the pressure-based solver are segregated algorithm and coupled algorithm. In the former, the governing equations are solved sequentially or segregated from one another, while in latter the momentum equations and continuity equations coupled together. The coupled algorithm converges the solution faster as compared to the segregated algorithm, but the memory requirement is more than the segregated algorithm. Therefore, to get more accurate results faster, coupled algorithm is used in this study [20].

3.2.2 Spatial Discretization Scheme

There are three methods to compute the gradient in Fluent[20]

- Green-Gauss Cell-Based
- Green-Gauss Node-Based
- Least Squares Cell-Based

In this study, a Green-gauss cell-based method is used to compute the gradient of the scalar at the cell faces and also to compute the secondary diffusion terms and velocity derivatives. This approach deals with fewer points over the domain as it

stores the solution at each cell-center thereby taking less memory than the node-center approach. The discrete form of this method is written as

$$(\nabla\phi)_{c0} = \frac{1}{\nu}\sum_{f} \bar{\phi}_f \, \vec{A}_f, \tag{3.1}$$

where $\bar{\phi}_f$ is the value of the scalar ϕ at the cell face centroid $c0$. The summation is over all the faces enclosing the cell. The face value, $\bar{\phi}_f$, is taken from the arithmetic average of the values at the neigboring cell centers, i.e.

$$\bar{\phi}_f = \frac{\phi_{c0} + \phi_{c1}}{2} \tag{3.2}$$

3.2.3 Viscous Model

Laminar viscous model is chosen in this study which specifies the laminar flow for the flat plate wing study. A part of this study which focuses on a validation with experimental results; a Spalart-Allmaras turbulent model is activated in simulation to reproduce the turbulent conditions of experiment.

3.2.4 Material

FLUENT Material Database has a list of available materials (fluid or solid or mixture) from which a desired material can be chosen. Also, the materials properties can be modified as per user's requirements. The fluid used for grid independence study is air with its density, 1.22 kg/m^3 and dynamic viscosity 1.580079 e-06kg/m-s. For the sensitivity analysis using design of experiments, the fluid properties of air changed depending on the Reynolds number and Strouhal number. These values are fed to FLUENT through an input file.

3.2.5 Boundary Conditions

Boundary condition is a condition that is required to be satisfied at all or part of the boundary of a region in which a set of differential equations is to be solved. Different boundary conditions are specified on different zones of the geometry. A velocity inlet condition is applied on the outer far-field while no-slip wall boundary condition is defined on the model. The required environment for the simulation like the velocity inlet, its magnitude and direction is set using Text Command Language (TCL) in Fluent.

3.2.6 Dynamic Mesh

The aim of this research is to study the flow analysis of a flapping wing for a cycle-averaged force production. Since flapping is a dynamic problem, a dynamic mesh is defined for the solver. An user-defined function (UDF) generates the required flapping path which is used to provide the dynamic mesh motion for the simulation which executes on demand by the input file.

Grid adaption is very important for dynamic mesh problems. It updates the mesh where needed, to resolve the flow field. This update can be actualized by three different methods in Fluent:

- Smoothing Methods
- Dynamic Layering
- Remeshing Methods

In the initial part of the research, Smoothing and remeshing methods were simultaneously applied for Grid adaptation. Spring/laplace/boundary Layer is a method available for smoothing which requires the spring constant and convergence tolerance values and remeshing was defined with maximum length scale and maximum

cell skewness values. This combination however did not give the desired adaptation and there was coarseness in the mesh.

So, in a different approach only smoothing was activated for grid adaptation using diffusion method. This method can be achieved either based on the boundary distance or cell volume. Boundary-distance-based diffusion allows the control of the diffusion of boundary into the interior of domain as a function of boundary distance. Lower diffusivity allows the absorption of more mesh motion which maintains the mesh quality near the moving boundary. Hence, this method was more suitable for the study of cyclic flapping wings with the diffusion parameter set to 2.

3.3 Governing Equations

ANSYS Fluent uses the finite-volume discretization method to solve the equations. In the finite-volume approach, the integral form of the conservation equations of mass, momentum and energy are applied to the control volume defined by a cell to get the discrete equations for the cell. The integral form of the continuity equation for steady, incompressible flow is

$$\int_S \vec{V} \cdot \hat{n} dS = 0 \tag{3.3}$$

The integration is over the surface S of the control volume and $\hat{n}$ is the outward normal at the surface. Physically, this equation means that the net volume flow into the control volume is zero.

A set of simultaneous algebraic equations needs to be solved as the discrete equations are applied for the cells in the interior of the domain while for the cells at or near the boundary, a combination of discrete equations and boundary equations are applied. Defining wrong boundary conditions will give entirely wrong result. When the numerical solutions are obtained for these equations within the tolerance range

fixed by the user, it is said grid convergence. Grid is also said to have converged solutions when the correct solutions become independent of the grid.

The Navier-Stokes and continuity equations provide the foundations for modeling fluid motion. The Navier-Stokes equations can be derived by considering the dynamic equilibrium of a fluid element. They state that the inertial forces acting on a fluid element are balanced by the surface and body forces. For incompressible flow, that is when the fluid density is constant, and ignoring body forces, the Navier-Stokes equations can be written as in equations 3.4,

$$\frac{\partial u}{\partial x}+\frac{\partial v}{\partial y}+\frac{\partial w}{\partial z}=0 \tag{3.4a}$$

$$\rho\left(\frac{\partial u}{\partial t}+u\frac{\partial u}{\partial x}+v\frac{\partial u}{\partial y}+w\frac{\partial u}{\partial z}\right)=-\frac{\partial p}{\partial x}+\mu\left(\frac{\partial^2 u}{\partial x^2}+\frac{\partial^2 u}{\partial y^2}+\frac{\partial^2 u}{\partial z^2}\right) \tag{3.4b}$$

$$\rho\left(\frac{\partial v}{\partial t}+u\frac{\partial v}{\partial x}+v\frac{\partial v}{\partial y}+w\frac{\partial v}{\partial z}\right)=-\frac{\partial p}{\partial y}+\mu\left(\frac{\partial^2 v}{\partial x^2}+\frac{\partial^2 v}{\partial y^2}+\frac{\partial^2 v}{\partial z^2}\right) \tag{3.4c}$$

$$\rho\left(\frac{\partial w}{\partial t}+u\frac{\partial w}{\partial x}+v\frac{\partial w}{\partial y}+w\frac{\partial w}{\partial z}\right)=-\frac{\partial p}{\partial z}+\mu\left(\frac{\partial^2 w}{\partial x^2}+\frac{\partial^2 w}{\partial y^2}+\frac{\partial^2 w}{\partial z^2}\right) \tag{3.4d}$$

In the above equations, 'u, v, w' are the velocity components in the 'x, y, z' directions, 'ρ' is the density, 'p' is the pressure, and 'μ' is the viscosity.

CHAPTER 4

GRID GENERATION AND FLAPPING TRAJECTORIES

4.1 Grid Generation

Pointwise V17.2 is computational fluid dynamics (CFD) meshing software and is used in this work. A good refined computational grid is a key for the accuracy of results obtained from the computational analysis. Grid is generated by creating domains using connectors. The number of points on the connectors defines the density of the grid. More points built a dense cell density which is commonly known as fine grid. A coarse mesh is where the density is less. A good mesh is when the density is more near the region where the flow is highly unsteady while coarser where it has fewer disturbances. It is also important not to make the mesh excessively dense because it requires more computational time and power.

2D Flat plate model as described in chapter 2 is meshed with O-type mesh for studying the grid independence study [figures:4.1(a), 4.1(b)]as well as the parametric study using DOE [figures:4.2(a), 4.2(b)]. The outer far-field is created and is dimensionalized. Dimensions are also set for the plate and domains are assembled to generate an unstructured grid. The grid is generated around the NACA 0012 airfoil for the validation case as shown in the [figures:4.2(a), 4.2(b)] using AFLR2 Software.

A volume grid is needed for a 3D elliptical plate. Domains are created on the plate and a spherical far-field is generated around the plate. For this study, to reduce the computational resources only one wing is meshed with a semi-spherical far-field. All these domains are assembled together to create an empty unstructured block. A

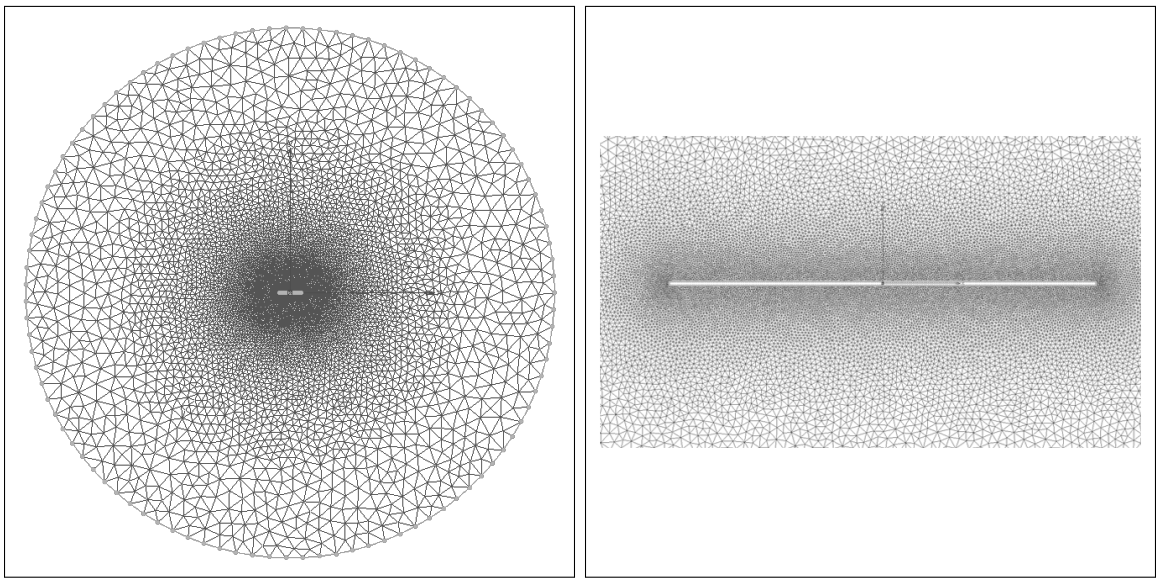

(a) (b)

Figure 4.1. Grids used in sensitivity analysis(a) Unstructured grid and (b) Grid near the flat plate.

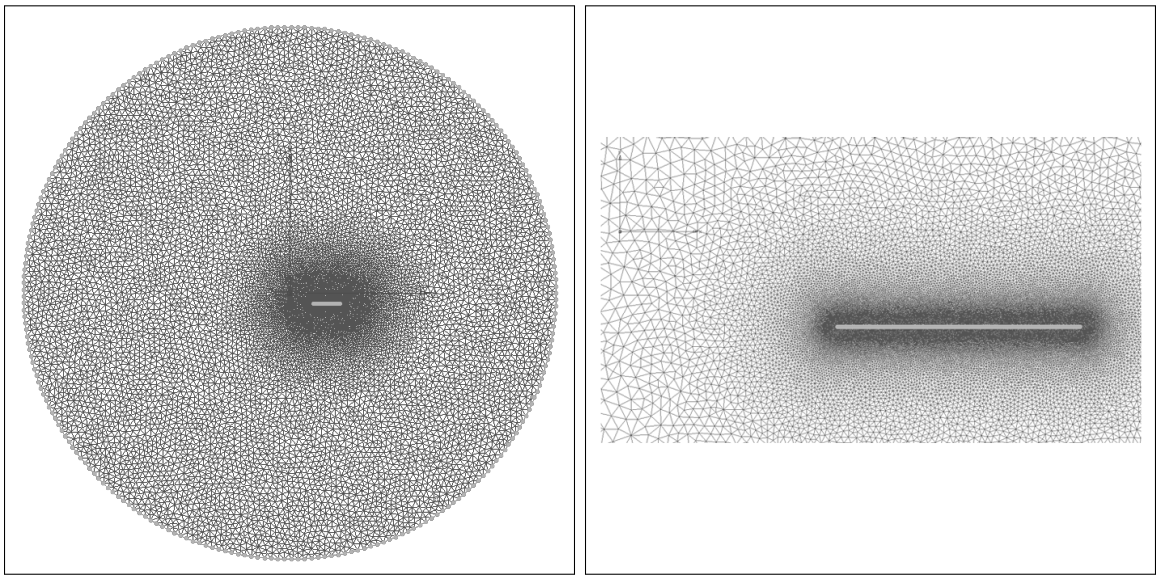

(a) (b)

Figure 4.2. Grids used in design of experiments(a) Unstructured grid and (b) Grid near the flat plate.

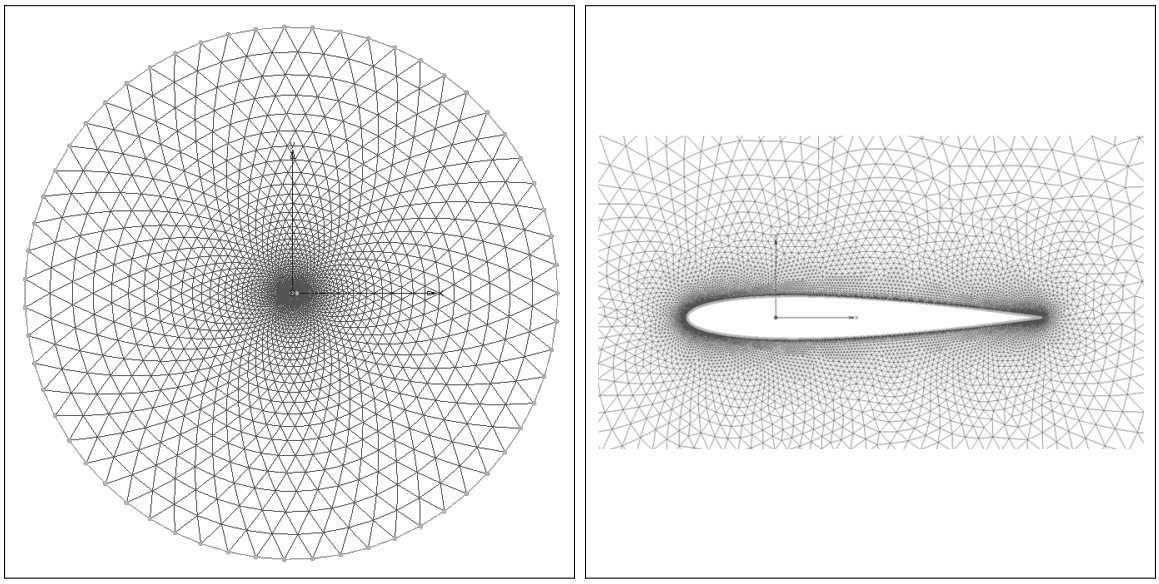

(a) (b)

Figure 4.3. Grids used in pitching case(a) Unstructured grid and (b) Grid near NACA 0012 airfoil.

block is then populated with T-Rex cells and initialized. The boundary conditions are set. A symmetric boundary condition is set on the plane of the hemisphere while a velocity inlet is defined for the semi-dome shape. A wall type boundary condition is set for the plate. The volume grid generated is as shown in the [figures:4.4(a), 4.4(b), 4.4(c)]

In this study, unstructured grid generation was preferred over structured, since unstructured grids reduce the overall complexity of the grid generation process. A better parallel performance is achieved with unstructured grids due to the ease of load balancing. Good grid adaptation properties for the moving mesh due to the motion of the flapping wing is also attained with unstructured grid. However, it is important to monitor the unstructured mesh schemes to check if there are high aspect ratio cells, since they add to the errors in the results. [3]

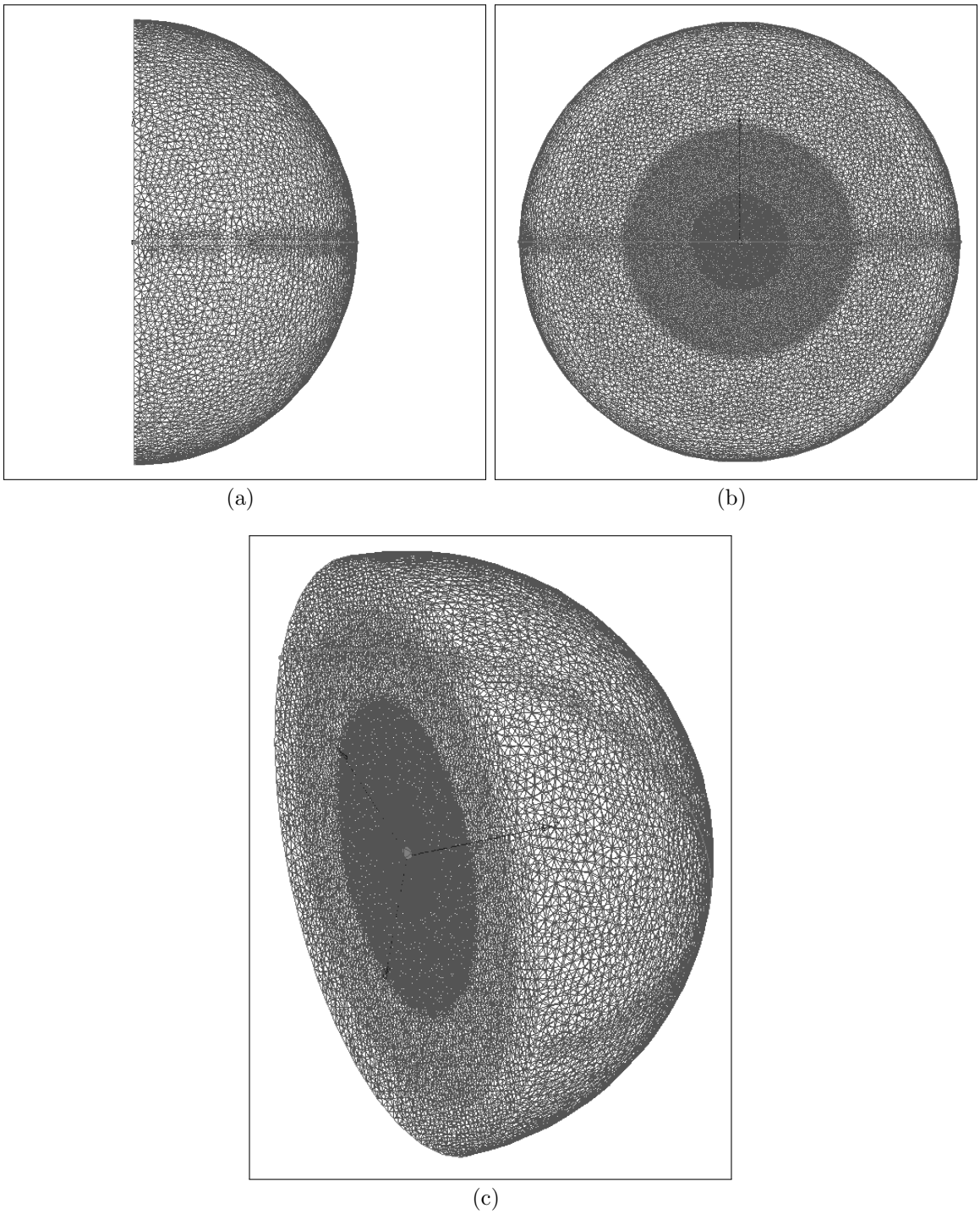

Figure 4.4. Grids used 3D Simulations(a) Unstructured volume grid (side view),(b) Grid at the symmetric plane of semi-spherical far-field and (c) Volume grid.

4.2 Flapping Trajectories

The aerodynamic forces generated by the insects and hence the bio-inspired MAVs depend on the motion of the wings. Insects follow many wing trajectories in nature while flapping. Two of these trajectories are considered in this study:

1. Straight path (2D and 3D)
2. Figure-8 motion

4.2.1 2D Straight path

Figures 4.5

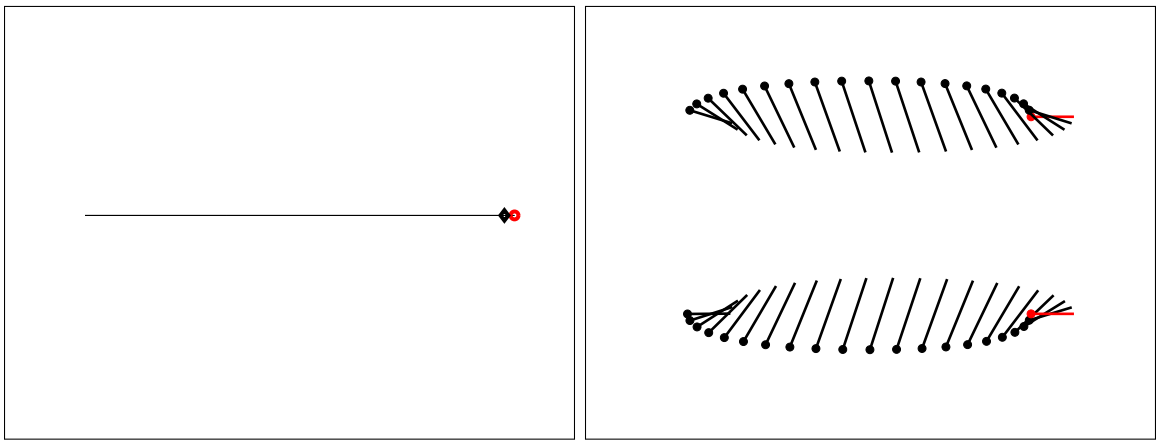

(a) (b)

Figure 4.5. 2D Straight flapping trajectory with(a) Flapping direction and(b) Instantaneous wing flapping positions.

4.2.2 3D Straight path

Figures 4.6

4.2.3 Figure-8 path

Figures 4.7

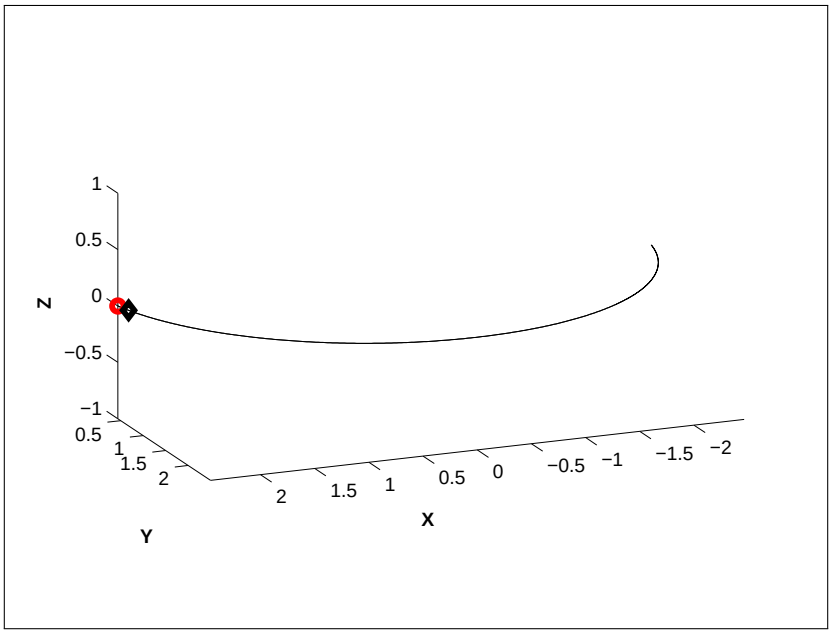

Figure 4.6. 3D Straight flapping trajectory.

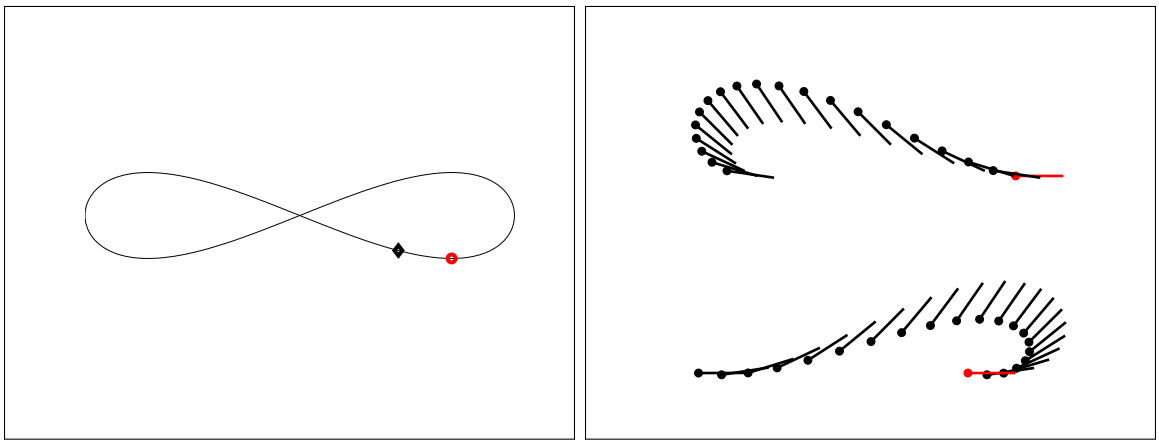

(a) (b)

Figure 4.7. Figure-8 flapping trajectory with (a) Flapping direction and (b) Instantaneous wing flapping positions.

4.2.4 Pitching case

Figures 4.8

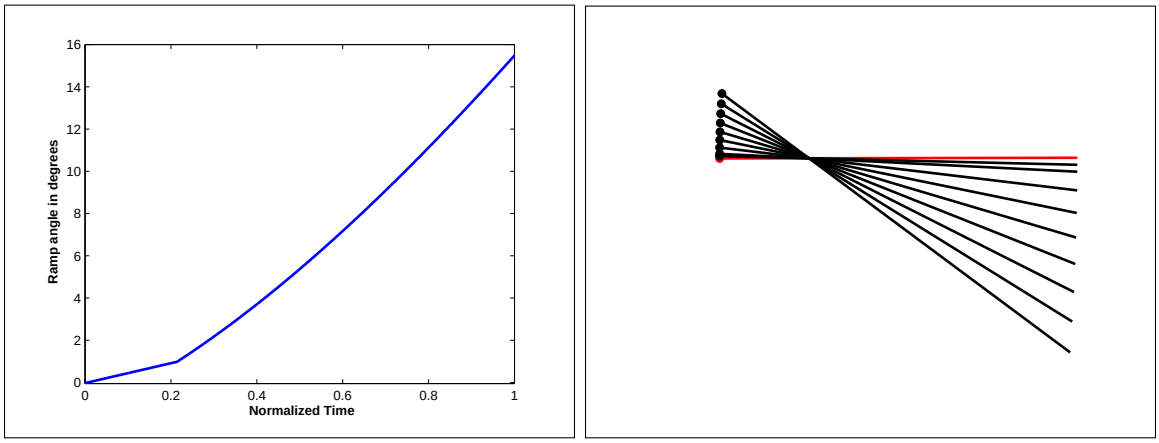

(a) (b)

Figure 4.8. Pitching trajectory with (a) Pitching direction and (b) Instantaneous wing pitching positions.

As seen in fig (a) for each of the trajectories, the circle and the diamond show the start and the direction of the wing stroke respectively. Fig (b) in each case shows the instantaneous wing positions during the two half strokes; the downstroke or the forward flapping motion of the wing, and the upstroke or the backward flapping motion. The circular head on the wing depicts the wing leading edge. All the paths were generated using parametric functions. The red color represents the initial and final position of the wing while the black shows the intermediate positions in flapping cycle.

4.3 Data Processing

Mesh is imported from Pointwise software into Fluent as a case file. User-defined functions and the native text command language are used to initialize all operations

to be performed within Fluent, including setting up the solver, defining the material of the fluid and boundary conditions, dynamic meshing, monitoring the forces for the unstructured moving mesh. Fluent is run in batch mode on the grendel machine using the distributed queueing software (DQS). An input file was used to feed the wing trajectory in the solver for mesh movement. The output files are generated after the solver finishes its task and writes out the data history for coefficients of lift and drag C_L and C_D respectively for the entire solver runtime. A C program was written to calculate the average lift, drag and moment coefficients (C_{Lavg} and C_{Davg} for the last flapping cycle. C_L and C_D data history was then imported to MATLAB for post-processing.

All the calculations in this study are non-dimensionalized. Observations from the previous study suggested that the average force coefficient values depend on the free stream velocity as well as the velocity generated due to wing flapping. These velocities are incorporated by defining two non dimensional parameters, the free stream Reynolds number and the local Reynolds number.

$$\text{Free Stream Reynolds number}, Re_f = \frac{\rho\ V_f\ c}{\mu} \tag{4.1}$$

$$\text{Local Reynolds number}, Re_l = \frac{\rho\ V_l\ c}{\mu} \tag{4.2}$$

where, ρ = density (kg/m^3) V_f = Free stream Speed (m/s) V_l = Local Speed $(m/s) = \omega L$ c = chord (m) μ = Dynamic Viscosity $(kg/m\text{-}s)$

Strouhal number, St gives the direct relation between the local and the free stream velocities. The Strouhal number 4.3 is defined as the ratio of local and free stream Reynolds numbers.

$$St = \frac{Re_f}{Re_l} = \frac{\omega L}{V_l} \tag{4.3}$$

where ω is the wing flapping frequency and L is the wing semi-span.

$$\text{Geometric function}, G = \frac{c}{L} \tag{4.4}$$

The non-dimensionalized forces were defined as below in equations 4.5 :

$$C_X = \frac{F_x}{0.5\ \rho\ \omega^2\ L^2\ c} \tag{4.5a}$$

$$C_Z = \frac{F_z}{0.5\ \rho\ \omega^2\ L^2\ c} \tag{4.5b}$$

C_X is in positive drag direction and C_Z is in positive lift direction.

CHAPTER 5

GRID INDEPENDENCE STUDY

5.1 Grid Independence Study

Dickinson et al.[18] developed a model for force coefficients seen in equation 5.1.

$$C_D\ (\alpha) = 1.92 - 1.55\ cos(2.04\alpha - 9.82) \tag{5.1a}$$

$$C_L\ (\alpha) = 0.225 + 1.58\ sin(2.13\alpha - 7.2) \tag{5.1b}$$

This model was valid only for the flapping in hover conditions. Also, this model is only a function of pitch angle (α).

Rege et al.[4] performed a parametric study to find the effect of factors other than pitch angle that influence the force generation. In his parametric study, he used different flapping trajectories made by 2D wing section of the MAV performed using CFD techniques with diameter of 10 times the chord length. His preliminary model was a function of Re_l, St and stroke angle of attack (α_S) as shown in equations 5.2.

α_S is the stroke angle of attack which is defined by the angle made by the free stream velocity with the flapping path as seen in the fig 5.1

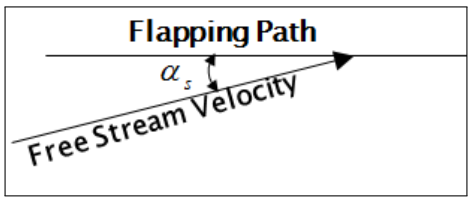

Figure 5.1. Stroke angle of attack (α_S) definition.

$$\text{Vertical force co-efficient}, C_{Zavg} = -247.4274 + 0.121Re_l + 27.941St + 3.454\alpha_S + 0.002Re_l^2 - 0.654St^2 + 0.241{\alpha_S}^2 - 0.024Re_l\alpha_S - 0.119St\alpha_S \tag{5.2a}$$

$$\text{Horizontal force co-efficient}, C_{Xavg} = 7289.5 - 7672St + 179St^2 \tag{5.2b}$$

Simulations at some the flow conditions for the sensitivity analysis data yielded undesirable results. This was because the grid adaptation was not uniform and grid in some regions became coarse as compared to other where the grid was too dense. There was no proper remeshing as seen in [fig 5.2]

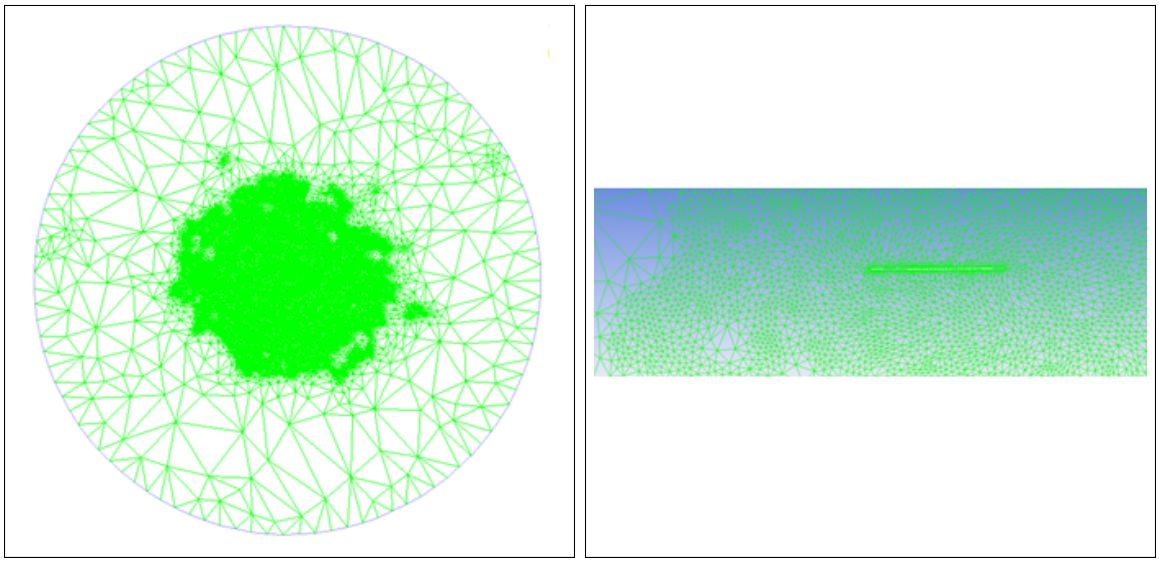

(a) (b)

Figure 5.2. Grids used by Rege et al.(a)and(b).

This study is solution to the problem discovered by Rege et al.. An exhaustive sensitivity analysis was done on outer boundary diameter to investigate cycle-averaged force co-efficients for 5^{th} flapping cycle. The main objective of this research was to

study the effect of grid sizes on the computational fluid dynamics solution and prove grid convergence with respect to the C_L and C_D values.

Mesh grid size is an important factor in numerical simulations because resolving of the flow motions depends significantly on the grid size to accurately describe the flows. Thus, finding or developing the right model that can satisfy the engineering solutions without the need of fine grid size (cheap computational cost) is one of the biggest challenges engineers are facing nowadays. As the grid size gets finer, it inflicts a high computational cost because of the type of models used, such as the direct numerical simulation (DNS). In contrast, if the grid size gets coarser, this leads to use the models developed by approximations such as the reynolds average navier stokes ($RANS$), which results poor description of the flow especially for the simulation of turbulent flows. Therefore, using the appropriate grid size is always crucial [21]. Typically, mesh is kept finer in the region where the flow is highly unsteady and coarser where there is relatively less disturbance. It is also essential to avoid unnecessary use of fine mesh to save on computational time and power [1]. Other than the quality of grid the computational analysis is also affected by the dimension of the grid. It is very important to choose an optimum diameter at the initial stages of the analysis. Dimension of the grid is defined by the diameter of the O-type grid.

The study started with grid generation in the Pointwise software as discussed in Section 4.1 . Fifteen different diameters where chosen from 15 to 50 times the chord length with an increment of 2.5 units. In all the cases, grid was generated in such a way that the cell density was more in the region near the flat plate and less dense as we move towards the circumference of the grid. The chord length was constant for all these cases. Once the grid was generated it was exported to the Fluent to study the effect of the straight path flapping motion of the flat plate at different far

field distances. The boundary conditions and the simulation environment were kept same to get unbiased results. A dynamic mesh was used to account for the 2-D wing flapping.

5.2 Results

The cycle-averaged forces obtained over the 51st cycle were compared for different far-field diameters and plotted in MATLAB to study the variation in the forces as the grid size changes.

In one part of the study different smoothing and remeshing methods were used. The values of coefficient of lift, drag and moment converged, but the grid quality after the simulation still demonstrated undesirable coarseness. To improve the quality of the grid, boundary distance diffusion smoothing technique was implemented to obtain the best diameter.

[Figures:5.3(a) and 5.3(b)] shows C_L and C_D versus different diameters respectively while table 5.1 shows percentage difference between two consecutive grid sizes. It can be seen that the solutions become independent of diameter at **30** times the chord length and also the percentage difference is least for both C_L and C_D. The aerodynamic forces do not depend on the number of cells in the grid after this size.

The quality of grid significantly improved which is seen in the figure 5.4

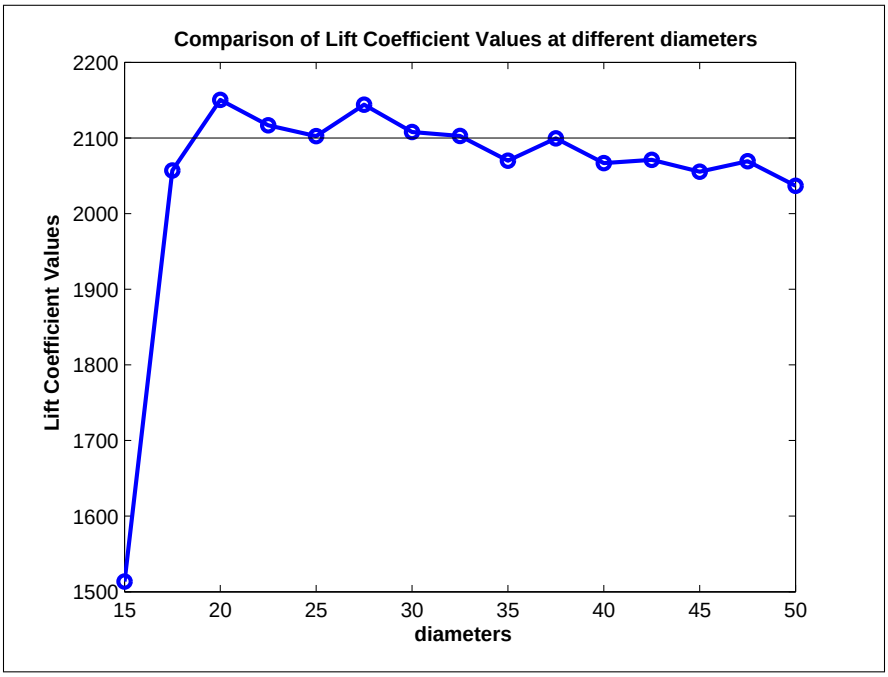

(a)

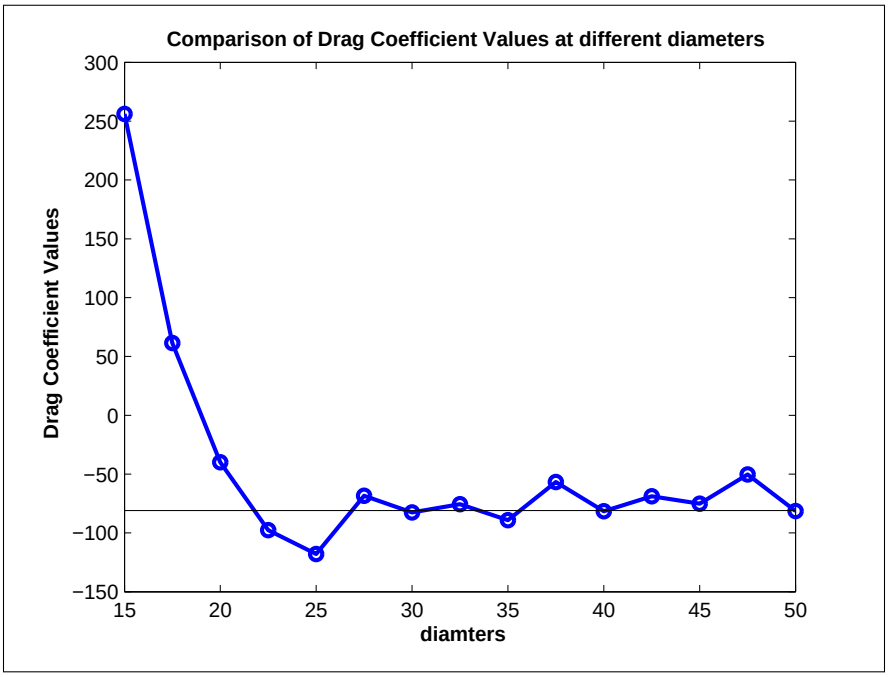

(b)

Figure 5.3. Fig (a) C_L versus diameter and fig (b) C_D versus diameter .

Table 5.1. Percentage difference between two consecutive grid sizes

Diameter Interval	C_L(in %)	C_D(in %)
15.0 - 17.5	26.42	-316.73
17.5 - 20.0	4.34	253.64
20.0 - 22.5	-1.58	59.03
22.5 - 25.0	-0.68	17.27
25.0 - 27.5	1.93	-72.64
27.5 - 30.0	-1.70	17.31
30.0 - 32.5	**-0.25**	**-9.39**
32.5 - 35.0	-1.58	15.20
35.0 - 37.5	1.40	-57.07
37.5 - 40.0	-1.58	30.46
40.0 - 42.5	0.20	-18.51
42.5 - 45.0	-0.75	8.375
45.0 - 47.5	0.66	-49.30
47.5 - 50.0	-1.59	38.22

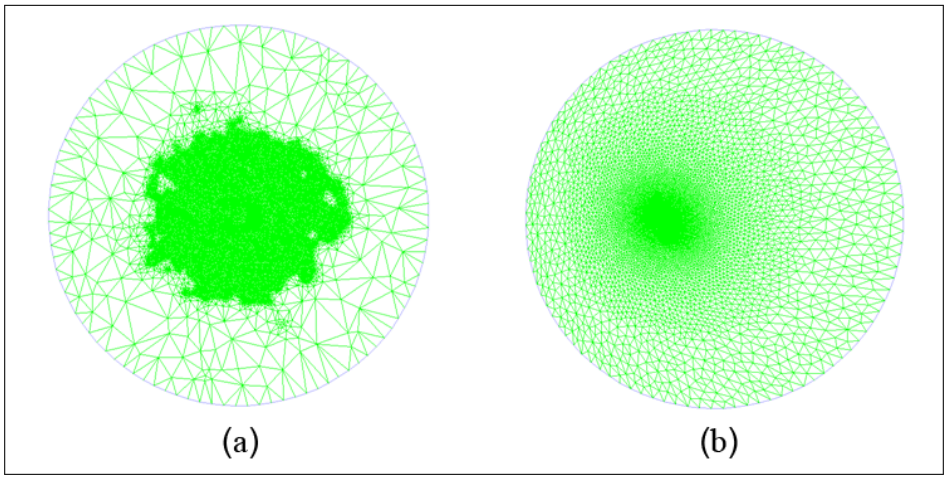

Figure 5.4. Comparison of grid fig (a) Grid adaptation with smoothing and remeshing method and fig (b) Grid adaptation with diffusion smoothing.

CHAPTER 6

EXPERIMENTAL VALIDATION

6.1 Experimental Validation

In this research, we are dealing with the flow over a wing section undergoing various flapping motions. Relying on the potential of the tool, a lot of research was conducted using ANSYS Fluent for the flapping wing of a micro air vehicle. But, there is always a need to develop the confidence in the results. This validation was done as a part of this work. The results of the simulations performed by the software were validated with the experimental results of the motion of NACA 0012 airfoil section, conducted by Advisory Group for Aerospace Research and Development (AGARD).

The figure 6.1 depicts the most fundamental algorithm to understand the concept of Validation. According to Roache, P.J.[22], validation is the process of determining the degree to which a model is an accurate representation of the real world from the perspective of the intended uses of the model or in simple words, validation provides evidence that the mathematical model accurately relates to experimental measurements.

In the experiment performed by AGARD (Mach Number, $M = 0.3$), airfoil is pitched about 0.25c axis taking a ramp motion from -0.03 deg to 15.54 deg. The time required for this motion is 0.01642 secs, this time interval from 0.0000 to 0.01642 is divided into 16 time steps. The experimental data presented in the AGARD report for ramp motion had 32 points.

Main aim of this validation is to obtain the same results using the CFD tool as that in the AGARD report. To reproduce the same results it is very important that

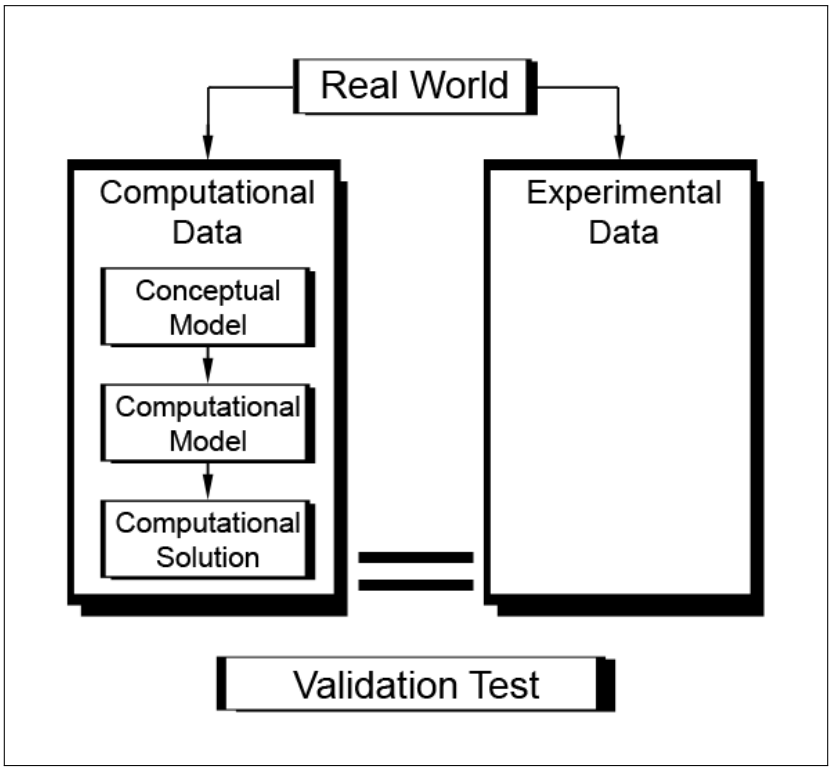

Figure 6.1. Concept of validation.

the flow conditions, boundary conditions, the geometry of the airfoil and the setup is same as that used in the report.

Firstly, it was necessary to generate a grid around NACA 0012 which was done using grid generation software, Pointwise. Unstructured grid was generated with 59545 triangular cells. Once the grid is generated it is exported as a Fluent case file. Because of the large number of computational procedures and settings, the Fluent Simulation was setup, initiated and post processed using a scripting language and Fluent text command language (TCL) as discussed in Section 4.3. User-defined functions (UDFs) were used to generate the motion and meshing. The ramp motion similar to that in the AGARD Report was generated using C language. The motion can be pictorially represented as in 4.8. The 16 time steps were curve fitted in two parts.

1. Linear fit between first two time steps

$$\alpha_P = 286.8576(t) - 0.03 \tag{6.1}$$

2. Polynomial fit from time steps 2 to 16

$$\alpha_P = -363594.5418(t^3) + 33160.5409(t^2) + 586.9399(t) - 1.4813 \tag{6.2}$$

where α_P is the angle of attack in deg for pitching airfoil and t is the time in secs.

After setting up the problem, the study was simulated with 1000 timesteps using Spalart-Allmaras Turbulent model because of high Reynolds number ($Re = 2.7\ e6$). The results generated at the end of simulations were imported to MATLAB and were plotted against the normal lift coefficients C_N from the AGARD Report.

A fellow graduate student applied NASA's FUN3D code to the same problem. The ramp motion was determined by applying a cubic spline to the experimental angle of attack. FUN3D simulations were accomplished using the same grid and the same number of time steps as the FLUENT simulations. Furthermore, the time accuracy was set to first order so that results from Fluent and FUN3D could be compared. FUN3D uses Anderson's artificial compressibility method[23] to numerically solve the incompressible Navier-Stokes equations.

6.2 Results

Fig 6.2 shows qualitative agreement between CFD predictions and the experimental data for the instantaneous lift coefficient throughout the lift-curve. Both Fluent and FUN3D tend to slightly under-predict C_N at extreme pitching angles.

6.3 Further Study

To investigate the possible reasons for variation in the CFD results, different simulations were done as discussed in table 6.3:

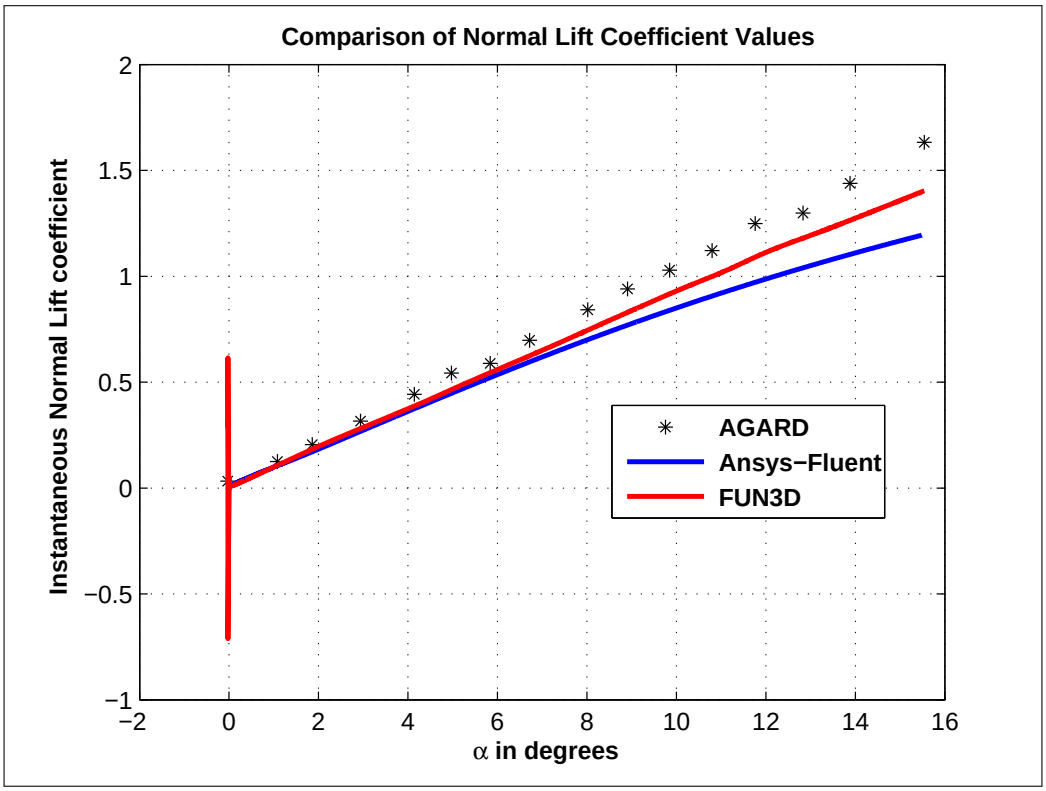

Figure 6.2. C_N v/s pitching angle : Validation results .

Run #	Solver	Order in time	Order in space	Convergence criteria	FVM method	Turbulence	Farfield BC	Curve fit	Number of iterations
1	Pressure based	1st	2nd	1.00E-03	Green Gauss cell based	Laminar	Velocity inlet	Liner+Poly nomial	50
2	Pressure based	2nd	2nd	1.00E-03	Green Gauss cell based	Turbulent	Velocity inlet	Liner+Poly nomial	50
3	Pressure based	2nd	2nd	1.00E-03	Green Gauss node based	Turbulent	Velocity inlet	Liner+Poly nomial	50
4	Pressure based	2nd	2nd	1.00E-03	Green Gauss cell based	Turbulent	Velocity inlet	Spline	50
5	Pressure based	2nd	2nd	1.00E-12	Green Gauss cell based	Turbulent	Velocity inlet	Liner+Poly nomial	100
6	Pressure based	2nd	2nd	1.00E-12	Green Gauss cell based	Turbulent	Velocity inlet	Liner+Poly nomial	50
7	Pressure based	2nd	2nd	1.00E-12	Green Gauss cell based	Turbulent with curvature corrections	Velocity inlet	Liner+Poly nomial	50
8	Pressure based	2nd	2nd	1.00E-12	Green Gauss cell based	Turbulent	Pressure-farfield	Liner+Poly nomial	50

Figure 6.3. Different simulation conditions.

1. Run 1. Fig 6.4

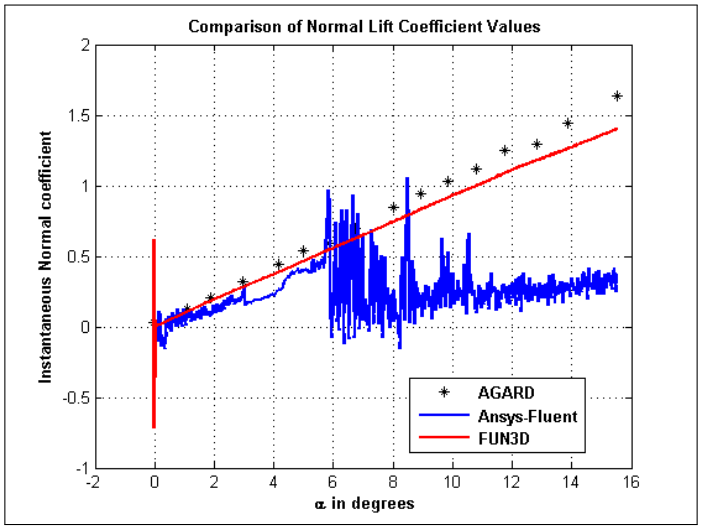

Figure 6.4. C_N v/s pitching angle : Validation results (Run 1).

- Here, the results of Fluent results have a lot of fluctuations in the force values because of the turbulence effects.

2. Run 2. Fig 6.5

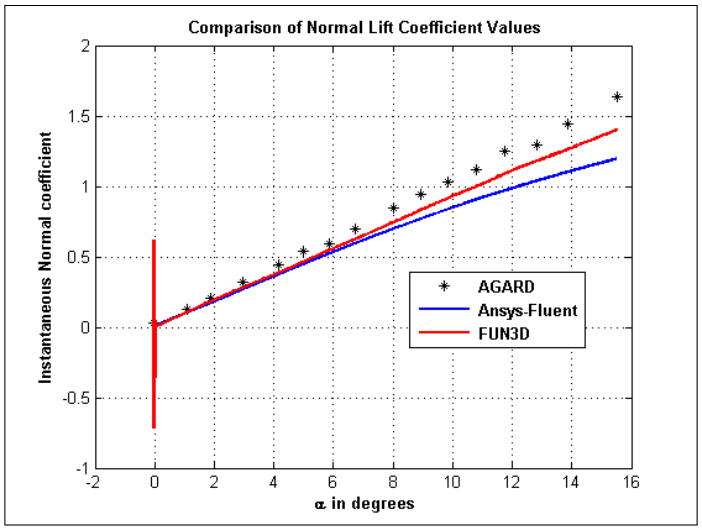

Figure 6.5. C_N v/s pitching angle : Validation results (Run 2).

- Here, the results of Fluent are independent of the degree of time and space. The results obtained are similar to that obtained before in Section 6.2.

3. Run 3.
   - The simulations were done in Fluent to reproduce the simulating conditions of the FUN3D CFD tool. But for this conditions the simulation did not complete (Non-positive volume exits).
4. Run 4. Fig 6.6

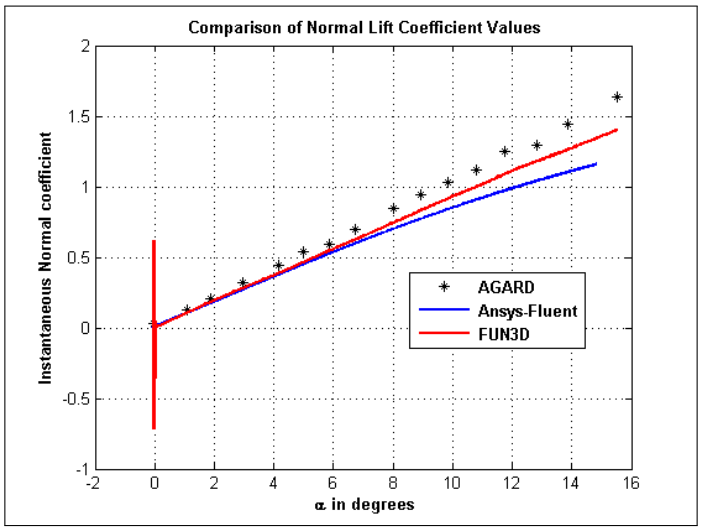

Figure 6.6. C_N v/s pitching angle : Validation results (Run 4).

- Here, the results of Fluent were not affected by the degree of curve fit for the pitching path and the results remain similar as in Section 6.2.
- The equation of the spline curve fit is as below:

$$\alpha_P = -2.875e6(t^3) + 1.013e5(t^2) + 18.69(t) - 0.0628 \qquad (6.3)$$

- The path of the spline can be represented as in fig 6.7
- Spline curve was incorporated because the FUN3D simulations follow a spline curve motion.

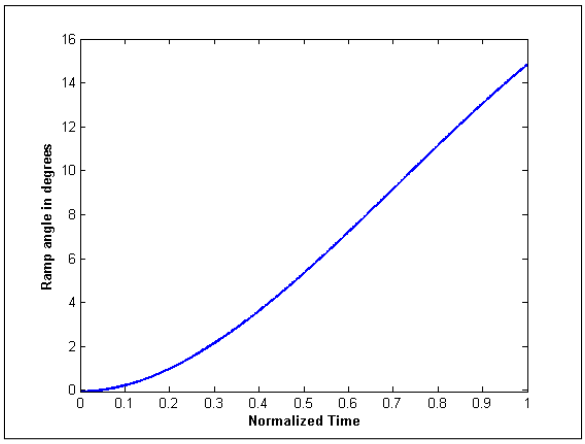

Figure 6.7. Pitching trajectory using Spline curve fit.

5. Run 5. Fig 6.8

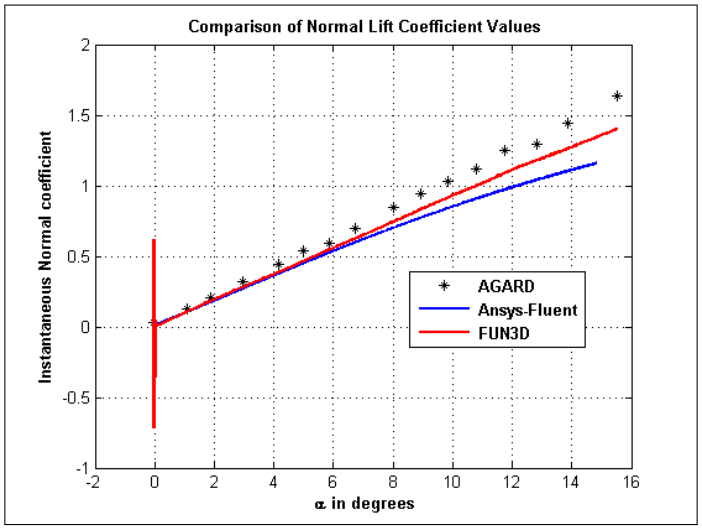

Figure 6.8. C_N v/s pitching angle : Validation results (Run 5).

- Here, the results of Fluent results are not affected by the number of iterations and the remain similar to that in Section 6.2.

6. Run 6. Fig 6.9

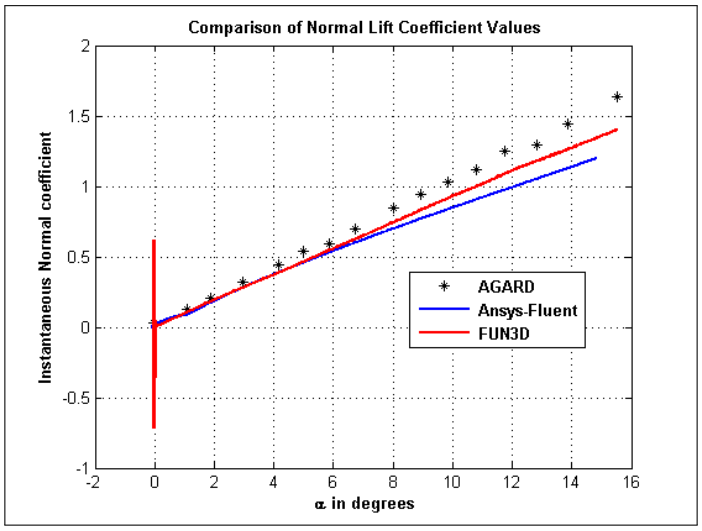

Figure 6.9. C_N v/s pitching angle : Validation results (Run 6).

- Here, the results of Fluent results are not affected by the convergence criteria from e-3 to e-12 and the remain similar to that in Section 6.2.

7. Run 7. Fig 6.10

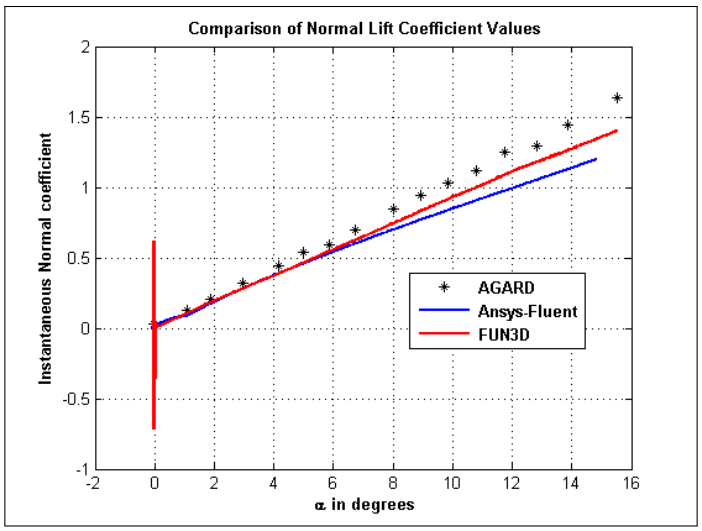

Figure 6.10. C_N v/s pitching angle : Validation results (Run 7).

- Here, the results of Fluent results are not affected by adding curvature corrections to turbulent model and the remain similar to that in Section 6.2.

8. Run 8
    - Solutions did not converge.

6.3.1 Conclusion

After using different methods, the best results were close to the results we already had in Section 6.2. Using different methods of solver did not change the results much. Also, at the same conditions of FUN3D, the results did not match. The reason for difference in the force values might be because of FUN3D uses a moving mesh and ANSYS Fluent uses grid adaptation method.

After checking the quality of grid after every timestep it can be seen that the quality of the grid is getting worse at every time step. So, this also might be one of the reasons for the difference in the values.

CHAPTER 7

SENSITIVITY ANALYSIS USING DESIGN OF EXPERIMENTS FOR FIGURE-8 FLAPPING PATH

7.1 Sensitivity Analysis Using Design of Experiments for Figure-8 Flapping Path

As an application of the grid study and after its validation, this sensitivity analysis was carried out. Sensitivity analysis done by Rege et al.[4] uses the parameters that affect the aerodynamic forces produced by flapping motion of a 2-dimensional wing of micro air vehicle. These parameters were nondimensionalized as mentioned in section 4.3. This research is an extension with an urge to find a new aerodynamic expression to study the flight dynamics of a bio-inspired flapping wing MAV. Previous work was done using the different values of parameters, like the Reynolds number (Re), Strouhal number (St) and the absolute Angle of attack (α in deg) while keeping the geometric function (G) constant throughout the study. A full factorial design of experiments was performed ie. $3^k = 27$ simulation runs, k = 3 because, 3 parameters were used in DOE, the details of which are shown in table 7.1 [4]

Table 7.1. Full factorial design of experiments

Parameter	Re_L	St	$\alpha_S(deg)$
maximum	31.88	28.5	5
mean	16.48	14.25	0
minimum	1.07	0.003	-5

The objective of this research was to help to obtain extended results by conducting more simulation runs in figure-8 flapping path which could help to develop a new aerodynamic expression.

In this research, authors are working on a larger data-set of parameter values mentioned above. Simulations are run for different combinations of parameter values and cycle-averaged force coefficient values C_{Zavg} and C_{Xavg} are obtained for each case. These values are then plotted against each parameter and results are analyzed. Rege et al. in [24] has done work in similar lines for Straight flapping path. Also, the data points chosen in this work are same as by Rege et al..

1. First run data points

Table 7.2. First run data points

Parameter	Value
St	[0.001, 0.01, 0.1, 1.0, 10.0, 100, 1000]
Re	[1.0, 50.0, 100.0, 150.0, 200.0]
G	[0.1, 1.0, 2.0, 4.0]
$\alpha_S(deg)$	[-40.0, -20.0, 0.0, 20.0, 40.0]

Number of combinations of simulation runs = $7 \times 5 \times 4 \times 5 = 700$

2. Second run data points

Table 7.3. Second run data points

Parameter	Value
St	[0.1]
Re	[1.0, 20.0, 40.0, 60.0, 80.0, 100.0, 120.0, 140.0, 160.0, 180.0, 200.0]
G	[0.4]
$\alpha_S(deg)$	[0.0, 3.0, 6.0, 9.0, 12.0, 15.0, 18.0, 21.0, 24.0, 27.0, 30.0, 33.0, 36.0, 39.0, 42.0, 45.0, 48.0, 51.0, 54.0, 57.0, 60.0, 63.0, 66.0, 69.0, 72.0, 75.0, 78.0, 81.0, 84.0, 87.0, 90.0]

Number of combinations of simulation runs = $1 \times 11 \times 1 \times 31 = 341$

The first run was done by selecting the parameters with a wide range of values and the results were studied. The second table concentrates on a more narrowed set of values and study was done in more detail with respect to the stroke angle of attack.

The aerodynamic forces required for an insect inspired MAV can be obtained using different trajectories of wing motion either to hover or to propel from one position to another. The most simplistic trajectories followed are the straight path and figure-8 path. This research will focus on the design of experiments using the parameters mentioned above following a figure-8 path discussed in section 4.2.3

Grid generation and flow solver setup is similar to that done for grid independence study for straight path as covered in section 5.1.

7.2 Results

The figures [7.1, 7.2] show the plot of cycle-averaged forces versus the stroke angle of attack (α_S) at different Reynolds numbers (Re) , while figures [7.3, 7.4] show the plot of average forces versus the Reynolds numbers (Re) at different angles of attack (α_S). These plots were obtained from the MATLAB code used by Rege et al. in their study.

The average vertical forces (C_{Zavg}) fig [7.1] has a similar trend at different Reynolds number, but after 55 deg the forces do not follow the same trend with increase in Reynolds number. There is a similar trend seen for average horizontal forces (C_{Xavg}) in fig [7.2]. (C_{Xavg}) does not follow the linearity at (α_S) higher than 55 deg.

After $Re = 40$, the values of the forces do not change and are constant except for few values of α_S. As seen in the plot for C_{Zavg} in fig 7.3, the forces are not following the linearity in pattern at particular combinations Re and α_S.

The many of the two cases are discussed below :

1. The brown curve for $Re = 60$ and $\alpha_S = 90$ there is a lot of variation in the forces values there is a lot of variation in the forces values .
2. The Navy Blue line for $Re = 60$ and $\alpha_S = 27$) there is a linearity seen in the values of C_{Zavg} .

The variations of the forces can be studied by studying the pressure contours for the flapping cycle.

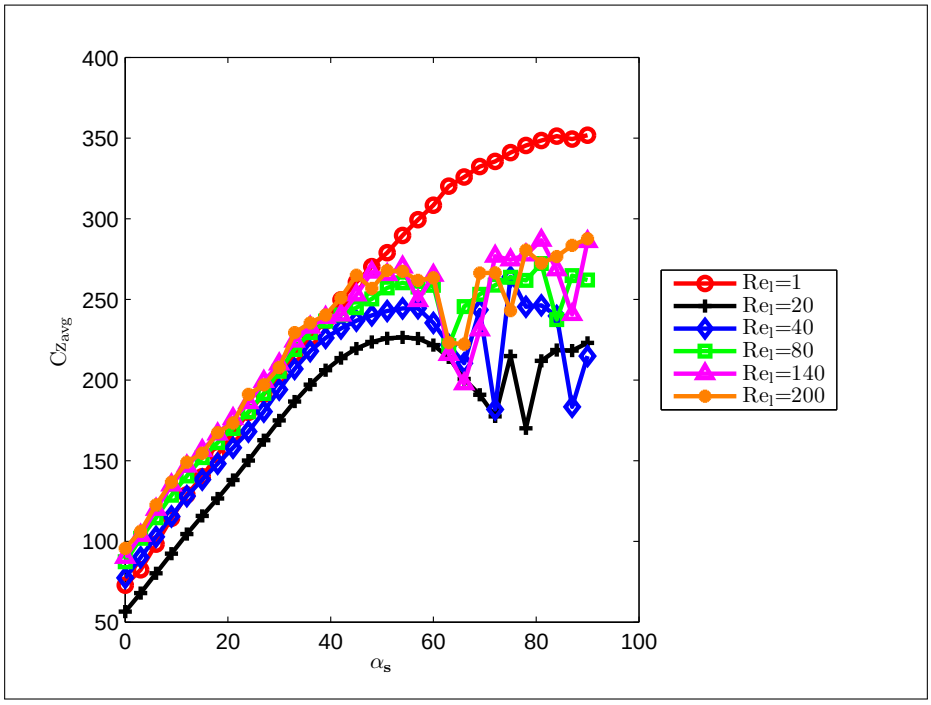

Figure 7.1. C_{Zavg} v/s α_S.

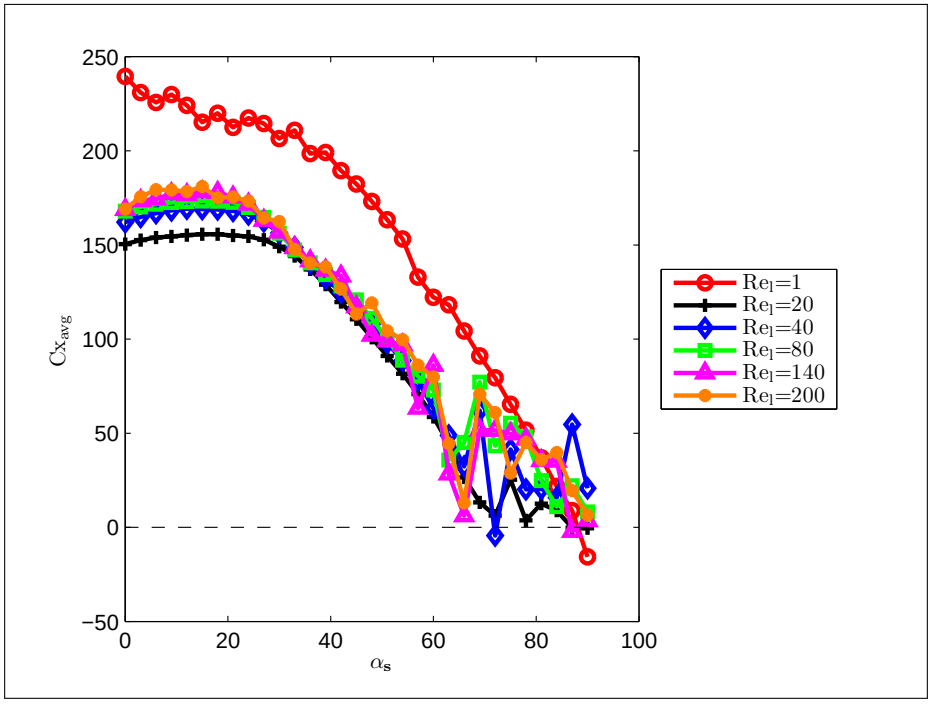

Figure 7.2. C_{Xavg} v/s α_S.

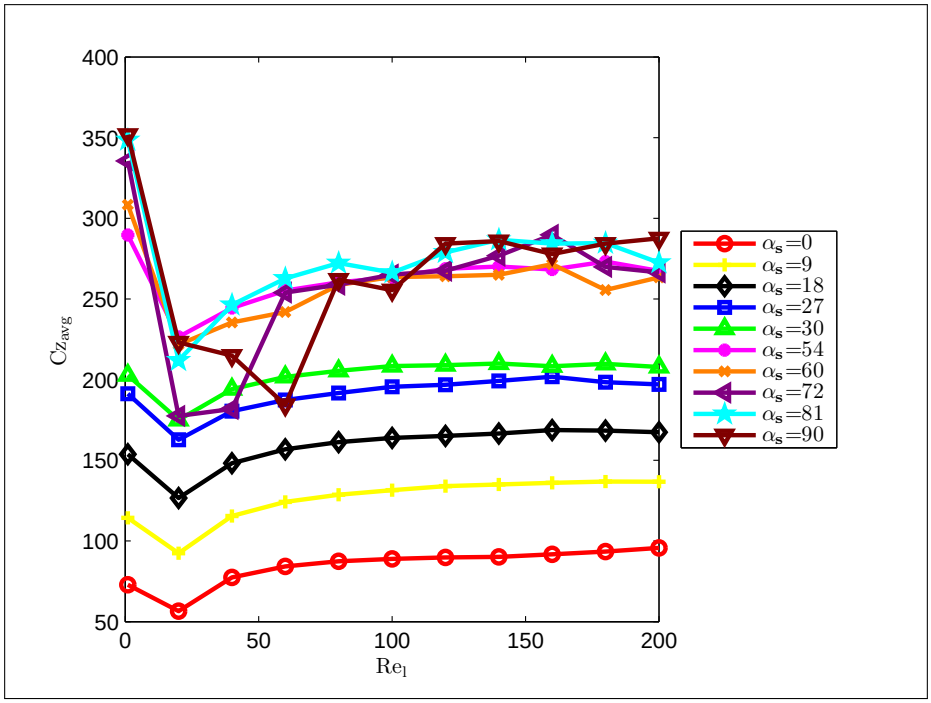

Figure 7.3. C_{Zavg} v/s Re_l.

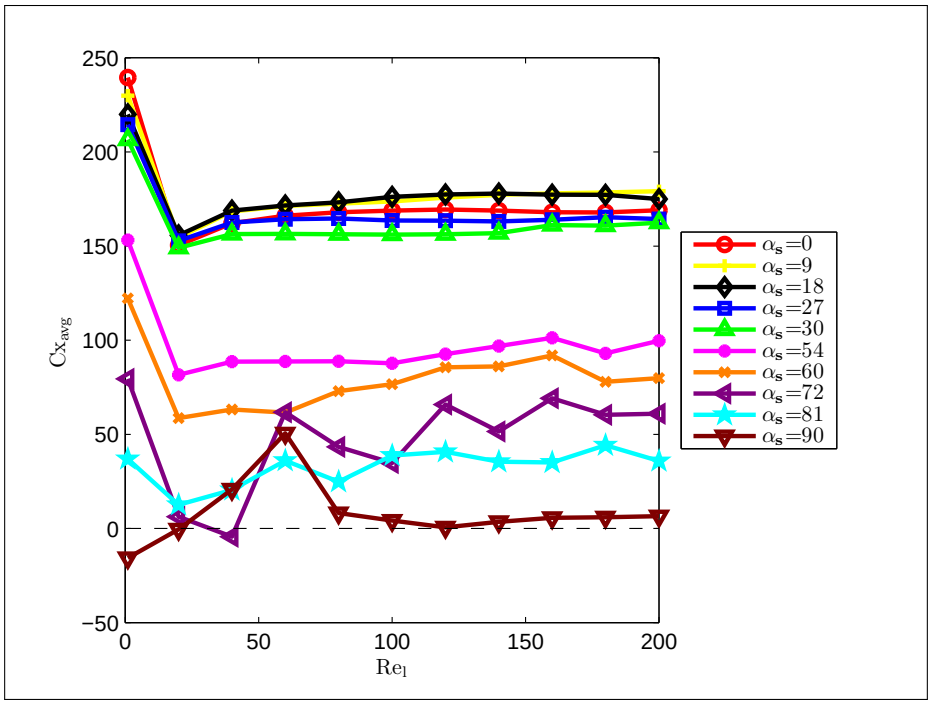

Figure 7.4. C_{Xavg} v/s Re_l.

CHAPTER 8

CONCLUDING REMARKS

8.1 Summary

The focus of this research study was to perform a study on grids in the CFD tool, ANSYS Fluent for the flow field over the flapping 2D flat plate wing section of a micro-flyer for cycle-averaged force production. The research was channelized in different parts:

1. Grid independence study for different far-field diameters.
2. Validation of CFD results with experimental data.
3. Sensitivity analysis and parametric study using design of experiments (DOE) for figure-8 flapping path.

The first part of the study started to obtain the best size of the grid by changing the far-field diameter. Straight path flapping motion was simulated with similar working conditions to obtain an unbiased result for different sizes of grid. The study of the simulation results indicated the best suitable size for the grid.

The next part was concentrated to develop the faith in CFD simulations. This was achieved by reproducing the experiment performed by AGARD for a pitching motion of airfoil NACA 0012. The first step was to collect the setup data of experiments and transfer it for computational analysis. The pitching about the 0.25c was replicated with the same working environment. The results of CFD showed good accordance with those presented in the AGARD Report. Also, an important point to keep in mind while conducting validation study is that the experimental results may always not be accurate because of various unknown errors.

The need to do a thorough sensitivity analysis on parameters like the Strouhal number, local Reynolds number, Stroke angle of attack and Geometric function. The interest of the research done by Rege et al. was to obtain a new aerodynamic model and to investigate the development of flow field and its effects on the production of aerodynamic forces. So, different combinations of simulations were performed for a Figure-8 motion of the wing section in this study. A collection of data set was used for this study and in all 1437 values of average coefficients of lift, drag and moment was obtained at different non-dimensionalized parameters. The average forces behave linearly on forces versus α_S graphs while they show a constant trend on Forces versus Re except for few α_S greater than 55 deg. It has to be noted that the figure-8 flapping could easily produce the lift but there was no significant production of thrust.

CFD is a great tool for such studies because simulating these humongous flow conditions those are difficult to reproduce in experimental test.

The last part of the study was to stretch the 2D study in the third dimension in spanwise direction. The study was started for the simplest case of flapping a thin elliptical plate in straight path. The volume grid was generated and exported to Fluent for the computational study of aerodynamic forces. Future work will be concentrated on continuing this work in the third dimension and study the flow analysis.

8.2 Future work

The validation of the results were done for a simple case of pitching at quarter-chord in 1st order in time. More accurate results can be predicted if a higher order in time is implemented using ANSYS Fluent V15. It would also be very interesting if more pitching and oscillating cases at low Reynolds Number are validated. This would build more confidence and establish better trust in the CFD results.

It would be a great to continue the sensitivity analysis for figure-8 and various flapping path, with a goal to obtain lift as well as higher value of thrust.

As mentioned in Section 8.1, immediate goal is to study the flow analysis for the 3D flapping wing following the straight path and obtain the cycle-averaged forces.

REFERENCES

[1] A. A. Rege, "CFD Based Aerodynamic Modelling To Study Flight Dynamics Of A Flapping Wing Micro Air Vehicle," Ph.D. dissertation, University of Texas at Arlington, 2012.

[2] F.-O. Lehmann and S. Pick, "The aerodynamic benefit of wing-wing interaction depends on stroke trajectory in flapping insect wings." *The Journal of experimental biology*, vol. 210, no. Pt 8, pp. 1362–77, Apr. 2007.

[3] A. A. Rege, B. H. Dennis, and K. Subbarao, "Parametric Study on Wing Flapping Path of a Micro Air Vehicle Using Computational Techniques," in *51st AIAA Aerospace Sciences Meeting including the New Horizons Forum and Aerospace Exposition*. Grapevine,TX: American Institute of Aeronautics and Astronautics, Jan. 2013, pp. 1–10.

[4] ——, "Sensitivity Analysis Of The Factors Affecting Force Generation By Wing Flapping Motion," in *Proceedings of the ASME 2013 International Mechanical Engineering Congress & Exposition*, San Diego, 2013, pp. 1–8.

[5] T. WEIS-FOGH, "Quick Estimates of Flight Fitness in Hovering Animals, Including Novel Mechanisms for Lift Production," *J. Exp. Biol.*, vol. 59, no. 1, pp. 169–230, Aug. 1973.

[6] R. Wood, "The First Takeoff of a Biologically Inspired At-Scale Robotic Insect," *IEEE Transactions on Robotics*, vol. 24, no. 2, pp. 341–347, Apr. 2008.

[7] S. P. Sane and M. H. Dickinson, "The control of flight force by a flapping wing: lift and drag production." *The Journal of experimental biology*, vol. 204, no. Pt 15, pp. 2607–26, Aug. 2001.

[8] W. Shyy, Y. Lian, J. Tang, H. Liu, P. Trizila, B. Stanford, L. Bernal, C. Cesnik, P. Friedmann, and P. Ifju, "Computational aerodynamics of low Reynolds number plunging, pitching and flexible wings for MAV applications," *Acta Mechanica Sinica*, vol. 24, no. 4, pp. 351–373, July 2008.

[9] Z. Jane Wang, "Two Dimensional Mechanism for Insect Hovering," *Physical Review Letters*, vol. 85, no. 10, pp. 2216–2219, Sept. 2000.

[10] R. Ramamurti and W. C. Sandberg, "A three-dimensional computational study of the aerodynamic mechanisms of insect flight," *J. Exp. Biol.*, vol. 205, no. 10, pp. 1507–1518, May 2002.

[11] A. R. ENNOS, "The Kinematics an Daerodynamics of the Free Flight of some Diptera," *J. Exp. Biol.*, vol. 142, no. 1, pp. 49–85, Mar. 1989.

[12] A. AZUMA, S. AZUMA, I. WATANABE, and T. FURUTA, "Flight Mechanics of a Dragonfly," *J. Exp. Biol.*, vol. 116, no. 1, pp. 79–107, May 1985.

[13] B. W. Tobalske, D. R. Warrick, C. J. Clark, D. R. Powers, T. L. Hedrick, G. A. Hyder, and A. A. Biewener, "Three-dimensional kinematics of hummingbird flight." *The Journal of experimental biology*, vol. 210, no. Pt 13, pp. 2368–82, July 2007.

[14] M. Sun and J. Tang, "Unsteady aerodynamic force generation by a model fruit fly wing in flapping motion," *J. Exp. Biol.*, vol. 205, no. 1, pp. 55–70, Jan. 2002.

[15] ——, "Lift and power requirements of hovering flight in Drosophila virilis," *J. Exp. Biol.*, vol. 205, no. 16, pp. 2413–2427, Aug. 2002.

[16] P. Bai, E. Cui, F. Li, W. Zhou, and B. Chen, "A new bionic MAVs flapping motion based on fruit fly hovering at low Reynolds number," *Acta Mechanica Sinica*, vol. 23, no. 5, pp. 485–493, Sept. 2007.

[17] J. M. Zanker, "The Wing Beat of Drosophila Melanogaster. I. Kinematics," *Philosophical Transactions of the Royal Society B: Biological Sciences*, vol. 327, no. 1238, pp. 1–18, Feb. 1990.

[18] M. H. Dickinson, "Wing Rotation and the Aerodynamic Basis of Insect Flight," *Science*, vol. 284, no. 5422, pp. 1954–1960, June 1999.

[19] AGARD, "Compendium of Unsteady Aerodynamic Measurements," AGARD, Advisory Group for Aerospace Research and Development, Tech. Rep., 1982.

[20] ANSYS Inc., *ANSYS FLUENT Theory Guide*, 14th ed. ANSYS, Inc., 2012.

[21] M. G. Gebreslassie, G. R. Tabor, and M. R. Belmont, "CFD Simulations for Sensitivity Analysis of Different Parameters to the Wake Characteristics of Tidal Turbine," *Fluid Dynamics*, vol. 2012, no. September, pp. 56–64, 2012.

[22] W. L. Oberkampf and T. G. Trucano, "Verification and Validation in Computational Fluid Dynamics," *Progress in Aerospace Sciences*, no. March, 2002.

[23] D. L. B. W. Kyle Anderson, Russ D. Rausch, "Implicit/Multigrid Algorithms for IncompressibleTurbulent Flows on Unstructured Grids," 1995.

[24] A. A. Rege, B. H. Dennis, and K. Subbarao, "Force Production by Wing Flapping: The Role of Stroke Angle of Attack and Local Reynolds Number," in *AIAA Aviation 2015 Conference*. Grapevine,TX: American Institute of Aeronautics and Astronautics, "forthcoming", pp. 1–7.

BIOGRAPHICAL STATEMENT

Born July 15, 1989, Navi Mumbai, India, Nitesh R. Rajput did his schooling in the same city. He received his Bachelor of Engineering (B.E.) degree with a major in Mechanical Engineering from Mumbai University, India, in 2011.

After undergraduate school, he started his M.S. degree program in Mechanical Engineering at the University of Texas at Arlington in Spring 2013. Over the course of M.S, he began working under Dr. Brian H. Dennis from Fall 2013 in the computational fluid dynamics laboratory on micro-flyer wings to study the flow analysis due the flapping motion of wings.

Nitesh has been a Teaching Assistant at UTA for the courses of Astronomy in Physics Department from Summer 2013 and also been involved in various co-curriculum and volunteering events on campus. In addition to that, he is also a student advisory member of a registered students' organization in UTA.